Intrazeolite Metal Carbonyl Kinetics: Substitution Reactions of $Mo(^{12}CO)_6$ in Sodium Zeolite Y

Heloise O. Pastore,[†,‡] Geoffrey A. Ozin,*[,‡] and Anthony J. Poë*

Contribution from the Lash Miller Chemical Laboratories, University of Toronto, 80 St. George Street, Toronto, Ontario, Canada M5S 1A1. *Received July 28, 1992*

Abstract: The first quantitative and detailed kinetic study of simple thermal reactions of a molecule encapsulated in a zeolite cavity is reported. Substitution reactions of $Mo(^{12}CO)_6$ with PMe_3 in the α-cages of a $Na_{56}Y$ zeolite host proceed cleanly to form *cis*-$Mo(CO)_4(PMe_3)_2$ by what are essentially pseudo-first-order dissociative and associative processes. Reactions with ^{13}CO proceed only by the dissociative path, which is 10^3 times faster than corresponding reactions in homogeneous solution. Dissociative substitution by PMe_3 is retarded by applied pressures of ^{12}CO, as expected, but it is also retarded to a significant extent by increased $Mo(CO)_6$ and PMe_3 loadings. Substitution by ^{13}CO is similarly retarded by increasing pressures of the entering ^{13}CO. The activation parameters, $\Delta H_d^* = 61 \pm 5$ kJ mol^{-1} and $\Delta S_d^* = -139 \pm 15$ J K^{-1} mol^{-1}, are unusual for a dissociative process but can be interpreted on the basis of structural information concerning pertinent reactant and product guests obtained mainly from FT-mid-IR, EXAFS, and DOR-MAS-NMR analytical methods. The kinetics data reveal that the α-cages of $Na_{56}Y$ provide precisely defined activating environments of a unique kind. From a coordination chemistry point of view, these "nanoreactors" appear to behave as macrospheroidal multidentate multisite anionic ligands (which we call "zeolates") toward extraframework charge-balancing cations to which metal carbonyl reactant, product, and ligand guests can become attached. The best model that emerges from this study pictures a supramolecular assembly of $Mo(^{12}CO)_6$ and PMe_3, ^{13}CO, or ^{12}CO, housed within the α-cage of $Na_{56}Y$, anchored to extraframework Na^+ cations, and subject to loading-dependent cooperative interactions. These interactions appear to control the extent of activation of $Mo(^{12}CO)_6$ through the degree of ordering (lock and key) of the $\{Mo(^{12}CO)_5\cdots{}^{12}CO\}^*$ dissociative transition state. All involve α-cage Na^+ anchoring interactions, probably together with some influence of oxygens of the six-rings. Substitution by PMe_3 can also occur by two associative paths, one that involves PMe_3 molecules chemisorbed to Na_{11}^+ ions in the nanoreactors, and another that we believe involves PMe_3 molecules physisorbed in the region of the 12-ring windows of the α-cages. Strikingly, these associative reactions are somewhat *slower* than corresponding reactions in homogeneous solution, and they are much less subject to loading effects than the dissociative reactions.

Introduction

A great deal is currently known about the static structure–bonding properties of a wide range of zeolite types.[1] Comparable details concerning occluded guests are beginning to emerge with the advent of a multiprong[2] solid-state approach to structure determination including such powerful methods as DOR-MAS-NMR, EXAFS, and RIETVELD PXRD.

Much information is also documented relating to the dynamic behavior of the zeolite host. These host lattice effects can be classified into oxygen-framework, T-atom, and extraframework-cation dynamics. The first[3] includes TOT bond making and breaking, $^{16}O/^{18}O$ isotope exchange, hydroxyl nest formation and healing, and adsorbate-induced structure transformations. The second encompasses dealumination, T-atom diffusion, and TO_4 motional effects.[4] The third involves intra- and intersite hopping, intra- and intercavity diffusion, and ion-exchange phenomena.[5]

Guest dynamics need to be categorized into two main classes. One concerns motional behavior within the void spaces, and the other focuses attention on reactivity patterns. The former contains effects such as intra- and intercavity diffusion, anchoring site acrobatics, and inter- and intramolecular exchange processes.[6] The latter depends on the class of guest, the type of intrazeolite chemistry, and whether stoichiometric or catalytic transformations are involved.[7] Considering the pervasive use of zeolites for a huge collection of size- and shape-selective chemical and catalytic processes, it is surprising to discover that quantitative studies, aimed at yielding activation parameters and mechanistic information, are essentially nonexistent in the open literature for virtually any kind of intrazeolite chemical reaction. One of the purposes of the present study is to begin to take a significant step toward improving this situation. Another goal of our research effort is to attempt to move beyond the static structure–bonding details derived from spectroscopic, diffraction, thermal, and microscopic methods and to start developing a type of "kinetic signature" for the intrazeolite reactivity patterns of different kinds of encapsulated guests. Through this approach one anticipates learning about intrazeolite annealing, ordering, anchoring, self-assembly, and cooperative phenomena involving reactants, transition states, and products, all subject to restricted geometry, size, and shape constraints.

The system selected as an archetype for our first investigation in this field is the ^{12}CO substitution of $Mo(^{12}CO)_6$–$Na_{56}Y$ by PMe_3 and ^{13}CO. A brief communication and a conference report of this work have been published recently.[8]

Experimental Section

Materials. The high-purity, crystalline sodium Y, denoted $Na_{56}Y$, with the unit cell composition $Na_{56}(AlO_2)_{56}(SiO_2)_{136}\cdot xH_2O$ was obtained from Dr. Edith Flanigen at UOP, Tarrytown, NY. To remove cation

† Present address: Instituto de Química, Universidade Estadual de Campinas, Campinas, S.P., Brazil.
‡ Advanced Zeolite Materials Group.

(1) Mortier, W. J.; Schoonheydt, R. A. *Prog. Solid State Chem.* **1985**, *16*, 5.

(2) Thomas, J. M.; Vaughan, D. E. W. *J. Phys. Chem. Solids* **1989**, *50*, 449. Fyfe, C. A.; Thomas, J. M.; Klinowski, J.; Gobbi, G. C. *Angew. Chem., Int. Ed. Engl.* **1983**, *22*, 259; Morrisson, T. I.; Iton, L. E.; Shenoy, G. K.; Suib, S. L. *J. Chem. Phys.* **1981**, *75*, 4086. Stucky, G. D.; Macdougall, J. E. *Science* **1990**, *247*, 669.

(3) Lehn, J.-M.; Meric, R.; Vigneron, J.-P.; Blanche-Waksman, I.; Pascard, C. *J. Chem. Soc., Chem. Commun.* **1991**, 62 and references therein.

(4) Yang, S.; Park, K. D.; Oldfield, E. *J. Am. Chem. Soc.* **1989**, *111*, 7278. Meier, W. M.; Groner, M. *J. Solid State Chem.* **1981**, *37*, 204. deMan, A. J. M.; van Beest, B. W. H.; Leslie, M.; van Santen, R. A. *J. Phys. Chem.* **1990**, *94*, 2524. Uytterhoeven, J. B.; Christner, L. G.; Hall, W. K. *J. Phys. Chem.* **1965**, *69*, 277. Cohen de Lara, E.; Delaval, Y. *J. Chem. Soc., Faraday Trans. 2* **1978**, *74*, 790. Khouzami, R.; Condurier, G.; Lefebvre, F.; Védrine, J.; Mentzen, B. *Zeolites* **1990**, *10*, 183.

(5) Ballmoos, R. *The ^{18}O-Exchange Method in Zeolite Chemistry: Synthesis, Characterization and Dealumination of High Silica Zeolites*; Verlag: Munich, 1981. McDaniel, C. V.; Maher, P. K. In *Zeolite Chemistry and Catalysis*; Rabo, J. A., Ed.; ACS Monograph Series 171; American Chemical Society: Washington, DC, 1976; p 285.

(6) Schoonheydt, R. A. *Proc. Int. Conf. Zeolites, 5th*; Rees, L. V. C., Ed.; Heydan: London, 1980; p 242. Jansen, F. J.; Schoonheydt, R. A. *J. Chem. Soc., Faraday Trans. 1* **1973**, *69*, 1338. Cremmers, A. *ACS Symp. Ser.* **1977**, *40*, 179.

(7) Angell, C. L. *J. Phys. Chem.* **1973**, *77*, 222. Ballinger, T. H.; Basu, P.; Yates, J. T., Jr. *J. Phys. Chem.* **1989**, *93*, 6758.

(8) (a) Ozin, G. A.; Özkar, S.; Pastore, H. O.; Poë, A. J.; Vichi, E. J. S. *J. Chem. Soc., Chem. Commun.* **1991**, *141*; (b) In *Supramolecular Architecture*; Bein, T., Ed.; ACS Symposium Series; American Chemical Society: Washington, DC, 1992; Vol. 499, p 314.

0002-7863/93/1515-1215$04.00/0

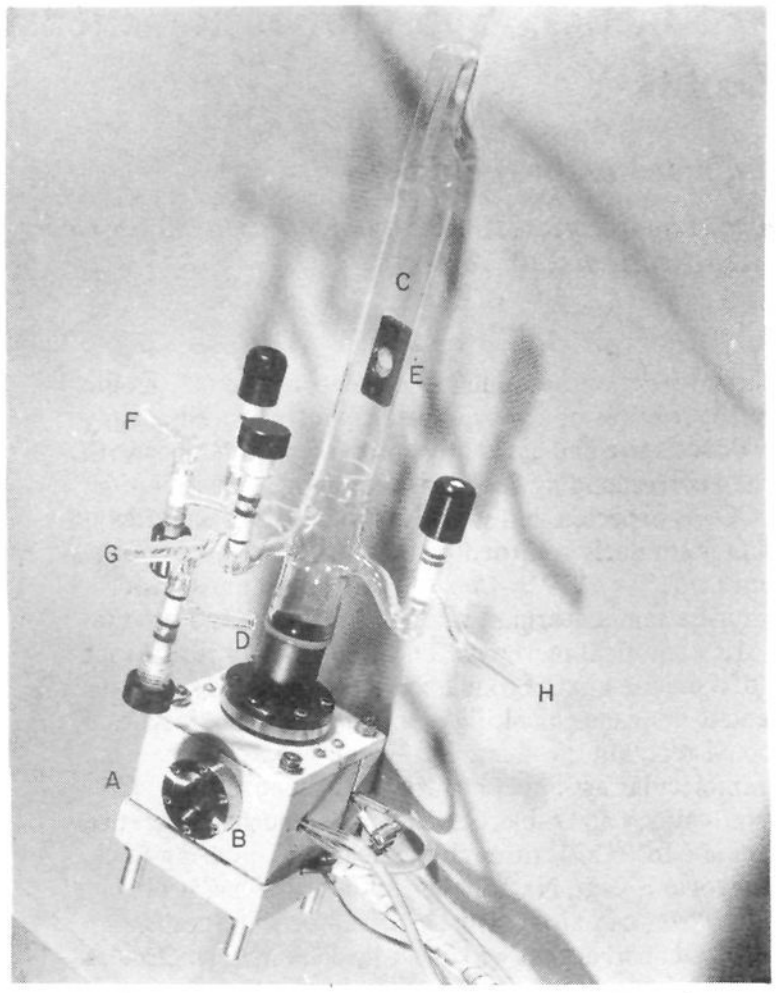

Figure 1. Mid-IR cell for in situ thermal treatments, loading of reactants, and kinetics measurements: (A) stainless-steel reaction chamber; (B) water/air-cooled NaCl windows; (C) quartz tube, where the dehydrations are done; (D) metal O-ring sealed flange; (E) stainless-steel sample holder; (F, and G) sublimation chambers; and (H) connection to vacuum/gas line.

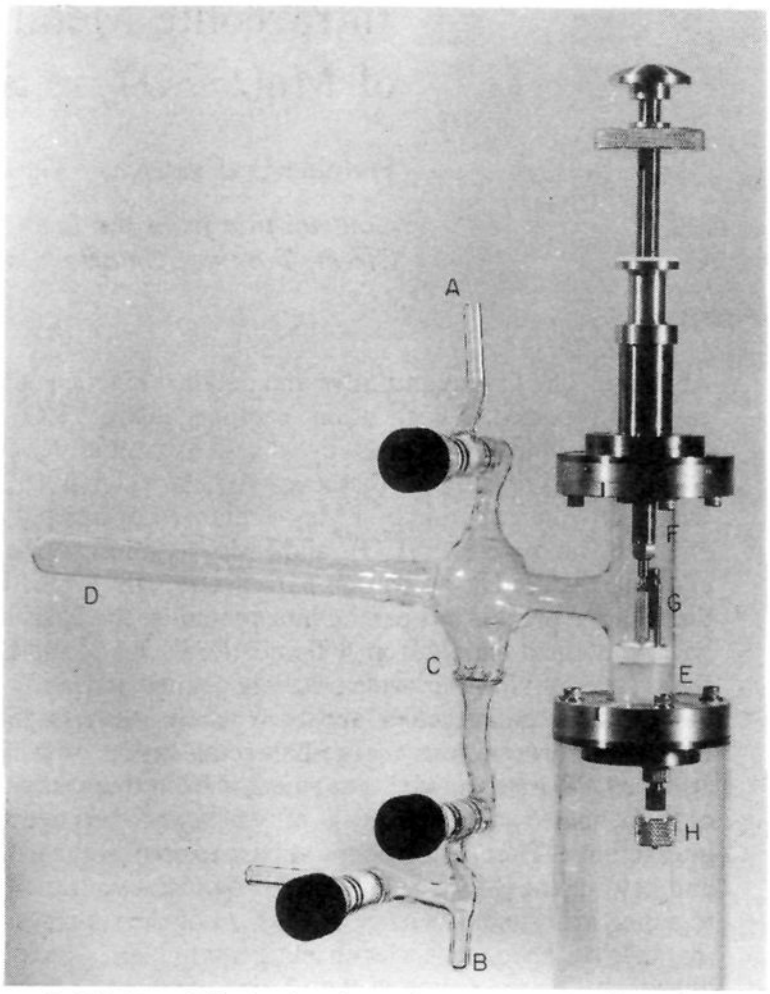

Figure 2. NMR cell for in situ thermal treatments, loading of reactants, and filling of the NMR zirconia rotor: (A) connection to vacuum/gas line; (B) reactant reservoir; (C) stainless-steel frit, where the zeolite is placed to be loaded with reactants; (D) quartz tube, where the thermal treatments are performed; (E) Teflon holder for the zirconia rotor; (F) plunger with the rotor cap; (G) mobile arm to compress the powder while loading the sample in the rotor; and (H) bottom part of G, with which this arm is moved.

defect sites, a sample of the calcined $Na_{56}Y$ was slurried with 0.01 M NaCl/0.01 M NaOH solution and washed until free of Cl^-. Samples were stored over saturated NH_4Cl solution to ensure a constant humidity. $Mo(^{12}CO)_6$ was purchased from Alfa Products, Wardhill, MA. Labeled ^{13}CO was obtained from Merck Sharp and Dohme Isotopes, Montreal, PQ. The adduct (trimethylphosphine)silver iodide, $(PMe_3{\cdot}AgI)_4$, was used as the source of PMe_3 (0.25 g of PMe_3/g of adduct) and was obtained from Aldrich, Milwalkee, WI. $Mo(CO)_5PMe_3$ and *cis*-$Mo(CO)_4(PMe_3)_2$ were synthesized according to literature procedures.[9]

Spectroscopic Cells. A specially designed mid-IR cell was used in this work for in situ treatment of samples and spectroscopic measurements. The kinetics cell (Figure 1) consists of a one-piece stainless-steel reaction chamber (A) with two water/air-cooled windows (B). The reactor is embedded in a specially built furnace which allows for heating the sample to the desired temperature. The reactor is joined, via a metal O-ring sealed flange (D), to a quartz tube (C) where all pretreatments are done. Thermal treatments in the quartz section of the cell can be carried out at temperatures up to about 500 °C, while the reactor can be used between room temperature and 200 °C. A zeolite wafer is placed into a stainless-steel holder (E), which can easily be moved into a space between the NaCl windows. A slit of the same size as the pellet holder assures that the sample does not move during measurements. The quartz end of the reactor has three T-shaped attachements: two sublimation chambers (F and G), and a connection (H) to a vacuum/gas line. The in situ loading NMR cell (Figure 2) consists of a double-crossed glass tube. The first cross arm connects the cell to a vacuum/gas line (A) and the reactant reservoir (B). The reactant reservoir can be either connected to a vacuum line or opened to the cell where the dried zeolite powder is held on the stainless-steel frit (C). The straight end of the cell is a quartz tube (D) where all the thermal treatments are performed. The zirconia rotor is housed in a Teflon holder (E) working also as a funnel. A multiple O-ring sealed cap for the rotor is attached to the plunger (F) and can be moved down to close the rotor after it has been packed. The cell also has a mobile arm (G) which helps to compress the powder properly in the rotor. It can be moved into position right above the rotor and pulled down using H. The far-mid-IR cell used in these studies was described elsewhere.[10]

Spectrometers. The mid-IR and far-IR spectra were taken on a Nicolet 20 SXB FTIR spectrometer. All spectra presented have been obtained by subtraction of the initial spectrum of the dehydrated zeolite from the spectrum of the sample after organometallic impregnation. ^{23}Na DOR-NMR spectra were recorded on an 11.7-T Chemagnetics CMX-500 spectrometer using a home-built probe described elsewhere.[11,25] The spinning speed was 5 kHz for the inner rotor and 500–700 Hz for the outer one. All samples were loaded into the inner rotor using rigorously anaerobic handling procedures. The experimental

(9) Darensbourg, D. J.; Kump, R. L. *Inorg. Chem.* **1978**, *17*, 2680. Bertrand, R. D.; Ogilvie, F. B.; Verkade, J. G. *J. Am. Chem. Soc.* **1970**, *92*, 1908.

(10) Baker, M. D.; Ozin, G. A.; Godber, J. *J. Am. Chem. Soc.* **1985**, *107*, 3033; *Catal. Rev.-Sci. Eng.* **1985**, *27*, 591.

(11) Wu, Y.; Sun, B. Q.; Pines, A.; Samoson, A.; Lippmaa, E. *J. Magn. Reson.* **1990**, *89*, 297.

(12) Arnesen, S. P.; Seip, H. M. *Acta Chem. Scand.* **1966**, *20*, 2711.

(13) Lee, P. A.; Citrin, P. H.; Eisenberger, P.; Kincaid, B. M. *Rev. Mod. Phys.* **1981**, *53*, 769.

(14) See figures in ref 8a.

(15) Özkar, S.; Ozin, G. A.; Moller, K.; Bein, T. *J. Am. Chem. Soc.* **1990**, *112*, 9575.

(16) Breck, D. W. *Zeolite Molecular Sieves*; R. E. Kieger Publishing Company: Malabar, 1984.

(17) Moller, K.; Bein, T.; Özkar, S.; Ozin, G. A. *J. Phys. Chem.* **1991**, *95*, 5276.

(18) Ozin, G. A.; Özkar, S.; Macdonald, P. *J. Phys. Chem.* **1990**, *94*, 6939. Ozin, G. A.; Malek, A.; Prokopowicz, R.; Macdonald, P.; Özkar, S.; Moller, K.; Bein, T. *Mater. Res. Soc. Symp. Proc.* **1991**, *233*, 109.

(19) Jelinek, R.; Özkar, S.; Ozin, G. A. *J. Phys. Chem.*, in press.

(20) (a) Fitch, A. N.; Jobic, H.; Renouprez, A. *J. Phys. Chem.* **1986**, *90*, 1311. (b) Goyal, R.; Fitch, A. N.; Jobic, H. *J. Chem. Soc., Chem. Commun.* **1990**, 1152.

(21) Zalewski, D. J.; Chu, P.; Tutunjian, P. N.; Lunsford, J. H. *Langmuir* **1989**, *5*, 1026.

(22) Godber, J.; Ozin, G. A. *J. Phys. Chem.* **1988**, *92*, 2841. Godber, J.; Baker, M. D.; Ozin, G. A. *J. Phys. Chem.* **1989**, *93*, 1409.

(23) Jelinek, R.; Chmelka, B. F.; Wu, Y.; Grandinetti, P. J.; Pines, A.; Barrie, B. J.; Klinowski, J. *J. Am. Chem. Soc.* **1991**, *113*, 4097.

(24) Welsh, L. B.; Lambert, S. L. *ACS Symp. Ser.* **1989**, *411*, 262. Engelhardt, G.; Michel, D. *High Resolution Solid-State NMR of Silicates and Zeolites*; Wiley: New York, 1987.

(25) Jelinek, R.; Ozin, G. A.; Özkar, S. *J. Am. Chem. Soc.* **1992**, *114*, 4907. Jelinek, R.; Ozin, G. A.; Özkar, S.; Pastore, H. O. *J. Phys. Chem.* **1992**, *96*, 5949. Jelinek, R.; Özkar, S.; Pastore, H. O.; Malek, A.; Ozin, G. A. *J. Am. Chem. Soc.*, in press.

(26) Yamazaki, T.; Watanuki, I.; Ozawa, S.; Ogino, Y. *Langmuir* **1988**, *4*, 433.

parameters used for observing ^{23}Na DOR-NMR spectra are the following: resonance frequency 132.28 MHz; 90° pulse length 11 μs; chemical shift reference material 0.1 M NaCl; pulse delay 0.5 s; aquisitions 500–1000 scans. All spectra were zero-filled to 2K data points, with 50-Hz Lorentzian broadening. In addition, ^{23}Na and ^{31}P MAS-NMR measurements at 7.0 T were carried out on a Chemagnetics CMX-300 spectrometer with a Chemagnetics MAS probe and rotor and 7.5-mm zirconia spinners run at speeds of ca. 3 kHz.[18] The following conditions for recording ^{23}Na MAS-NMR spectra were used: resonance frequency 79.2 MHz; 90° pulse length 5 μs; pulse delay 2 s; aquisitions 500–1000 scans. ^{31}P MAS-NMR spectra of solid samples were recorded at a resonance frequency of 121.3 MHz: 90° pulse length 4.1 μs; pulse delay 2 s; aquisitions 500–1000 scans.

EXAFS data were collected at the National Synchrotron Light Source (Brookhaven National Laboratory, Upton, NY) on beam line X-11A.[27] The monochromator was equipped with a Si(330) crystal pair, which was not detuned since synchrotron radiation harmonics do not cause interferences at energies near 20 keV. The data were obtained in transmission mode by using a pair of GSK Scientific ionization detectors filled with krypton (sealed, post sample detector) and flowing argon (pre sample detector), respectively, both at atmospheric pressure. All samples were cooled to about 100 K before spectra were taken. For all samples and the reference (bulk crystalline $Mo(CO)_6$, in which the Mo–C distance as determined by crystallography[12] is 2.063 Å), the Mo K edge at 20.000 keV was scanned beginning at 200 eV before, and ending at about 1300 eV above, the edge. The monochromator energy origin was calibrated using a 5-μm molybdenum foil.

Loading Determinations. About 20 mg of size-sieved zeolite crystals was pressed into a self-supporting wafer having a diameter of 16 mm by applying a pressure of 5 tons/in.^{2} for 10 s. The disk was secured in the stainless-steel holder and placed in the quartz part of the cell. The wafer was thermally dehydrated under dynamic vacuum by using an Omega series CN-2010 programmable temperature controller according to a preset program: 25–100 °C over 3 h, 4 h at 100 °C, 100–450 °C over 5 h, and 2 h at 450 °C. Dehydration was followed by calcination in a static atmosphere of 300–350 Torr of O_2 at 450 °C for 1 h, which was followed by pumping at this temperature for 30 min. The degree of dehydration was judged by the flatness of the base line in the mid-IR ν_{OH} stretching and δ_{OH} deformation regions, 3400–3700 and 1600–1650 cm^{-1}, respectively. When a sufficiently dehydrated sample was obtained, the wafer was moved into position above the entrance to the sublimation chamber and loaded with PMe_3, $Mo(CO)_6$, and $Mo(CO)_5PMe_3$ in the infrared cell to amounts controlled by opening the appropriate valve for a fixed time and measured by the absorbance of the bands at 1437, 2123, and 2068 cm^{-1}, respectively. The wafers were then analyzed for their content in phosphorus and molybdenum by SEM-EDX (Imagetec) and in molybdenum by neutron activation analysis (the University of Toronto Slow Poke facility). Linear plots of absorbance vs phosphorus or molybdenum content were obtained and used as loading calibrations in later experiments.

The maximum loading of chemisorbed trimethylphosphine was determined by introducing the vapor of the compound into the zeolite wafer in the cell and pumping at room temperature until the absorbance of the band of intrazeolite PMe_3 at 1437 cm^{-1} remained constant. This sample was then analyzed for the content of phosphorus.

NMR Measurements. The samples for the NMR studies were prepared as follows: 300 mg of size-sieved $Na_{56}Y$ was placed in the quartz end of the cell shown in Figure 2 (D) and thermally dehydrated, according to the program described above. The $Na_{56}Y$ powder was then collected on the frit (C), and a predetermined amount of $Mo(CO)_6$ and/or PMe_3 was sublimed into the cell. For the preparation of $\{Mo(CO)_4(PMe_3)_2\}$–$Na_{56}Y$, a known amount of $Mo(CO)_6$ followed by PMe_3 was introduced into dehydrated $Na_{56}Y$. In this case, after the addition of the reactants, the powder was moved back to the quartz section of the cell and heated at 65.8 °C for 2 h. The sample was moved toward the Teflon holder (E) where the rotor was placed, and gradually the powder was packed and pressed into the rotor with the aid of a plunger (G). The anaerobically sealing rotor cap was then pushed into place.

EXAFS Measurements. Samples for analysis by EXAFS were embedded under an inert atmosphere in a mixture (50 wt % each) of reagent grade octacosane and hexatriacontane and then pressed into wafers of uniform 10-mm thickness inside aluminum cells. Following this, 25-μm-thick Kapton windows were affixed to the cells using high-vacuum-grade epoxy resin. The amount of material embedded in each cell was chosen so as to give a total X-ray absorption of about 1.5 at the Mo K edge (20.000 keV). The data were analyzed according to standard methods,[13] and the structural parameters (interatomic distances, coordination numbers, static disorder, and inner potentials) of the samples were obtained by simultaneous least squares fitting of each filtered, back-transformed data set using phase and amplitude functions extracted from the reference compound.

Kinetics Measurements. Suitably dehydrated wafers (ca. 20 mg) of $Na_{56}Y$ were loaded with $Mo(^{12}CO)_6$ and PMe_3 as described above, the PMe_3 loading generally being in molar excess compared with that of $Mo(^{12}CO)_6$.

The addition of gaseous compounds, ^{12}CO and ^{13}CO, was performed after the occlusion of organometallics and, where appropriate, the trimethylphosphine. Pressure-dependent kinetics experiments were performed in the range from 25 to 650 Torr.

After all the reactants had been added to the zeolite, the cell was held horizontally, the wafer located in the quartz end of the cell, and the reactor heated to the reaction temperature for 1 h to allow for stabilization of the reactor temperature. The sample was then placed between the NaCl windows of the kinetics cell for measurements. At each temperature studied, time was allowed for the wafer to reach the reaction temperature.

Rate data were obtained by monitoring changes in the intensity of the IR band at 1975 cm^{-1} due to $Mo(^{12}CO)_6$. All the reactions studied showed very clean isosbestic points in the IR spectra,[14] and no further spectroscopic changes were observed after completion of the initial reaction. In all cases values of A_∞ were very small when compared to the initial A_0 values. Plots of $\ln [(A_t - A_\infty)/(A_0 - A_\infty)]$ versus time were linear for about 85–90% of the reaction.[14]

Results

Nanoreactor Loading. Quantitative adsorption experiments demonstrate that saturation loading of $Mo(^{12}CO)_6$ from the vapor phase into $Na_{56}Y$ yields samples containing 2 $Mo(^{12}CO)_6$/α-cage or 16 $Mo(^{12}CO)_6$/unit cell, denoted by $16\{Mo(^{12}CO)_6\}$–$Na_{56}Y$.[15] The population n of occluded $Mo(^{12}CO)_6$ guests per unit cell can be controlled to any value in the range $0 \leq n \leq 16$. Similar uptake experiments conducted for PMe_3 defined saturation loading values under vacuum (i.e., chemisorbed PMe_3) that are double that of $Mo(^{12}CO)_6$, namely, $32\{PMe_3\}$–$Na_{56}Y$. Additional, physisorbed PMe_3 molecules can be occluded in each unit cell to give a total of almost $56\{PMe_3\}$–$Na_{56}Y$ in the absence of an applied vacuum. At half-saturation loading values of $Mo(^{12}CO)_6$, the adsorption capacity remaining for chemisorbed PMe_3 was determined to be half of its normal value, yielding samples denoted by $8\{Mo(^{12}CO)_6\},16\{PMe_3\}$–$Na_{56}Y$; further sublimation of PMe_3 can yield samples approaching $8\{Mo(^{12}CO)_6\},40\{PMe_3\}$–$Na_{56}Y$.

Organization of $Mo(^{12}CO)_6$ and PMe_3 in the Nanoreactors. Crystallographic studies of $Na_{56}Y$ have established the existence of cations at sites II and III in the supercage.[16] The α-cage six-ring sites II are always the most highly populated, with roughly four cations per supercage, creating what appears to be a "tetrahedral ion trap" for occluded guests. In the case of $n\{Mo(CO)_6\}$–$Rb_{56}Y$ and $n\{W(CO)_6\}$–$Na_{56}Y$, EXAFS,[15,17] FT-mid-far-IR,[18] and ^{23}Na MAS-DOR-NMR[19] structure analysis defines the presence of the hexacarbonylmetal(0) guest, anchored to, and locked between, two adjacent site II cations. A maximum of 2 $M(CO)_6$ guests oriented orthogonally with respect to each other can be housed in the α-cage of $Na_{56}Y$. These structures are illustrated in the Chem-X space-filling model shown in Figure 3B,D.

^{31}P MAS-NMR, ^{23}Na MAS-DOR-NMR, and FT-mid-far-IR spectroscopic analysis of $m\{PMe_3\}$–$Na_{56}Y$ favors a scheme in which each PMe_3 is coordinated to an α-cage Na^+ ion. At saturation loading under vacuum it is therefore likely that the four PMe_3 molecules are chemisorbed to the four tetrahedrally disposed site II Na^+ ions, as illustrated in the Chem-X space-filling model shown in Figure 3A. This structure is somewhat analogous to that determined by neutron diffraction for $m\{C_6H_6\}$–$Na_{56}Y$.[20a] The additional PMe_3 molecules that can be adsorbed in the absence of an applied vacuum are only physisorbed, and they most probably reside in the vicinity of the four 12-ring entrance windows to the supercage of $Na_{56}Y$. In this they resemble the situation shown[20] by neutron diffraction data for benzene and pyridine in $Na_{56}Y$, and physisorbed PMe_3 has also been shown[21] by ^{31}P MAS-NMR to exist in $H_{56}Y$ under similar loading conditions.

Following occlusion of $Mo(CO)_6$ vapor in $Na_{56}Y$, fully equilibrated (annealed) samples can be produced. These are best described[15] as *trans*-ZONa···(OC)$Mo(CO)_4$(CO)···NaOZ per-

(27) Enzel, P.; Ozin, G. A.; Özkar, S.; Pastore, H. O.; Prokopowicz, R. *J. Phys. Chem.*, submitted.

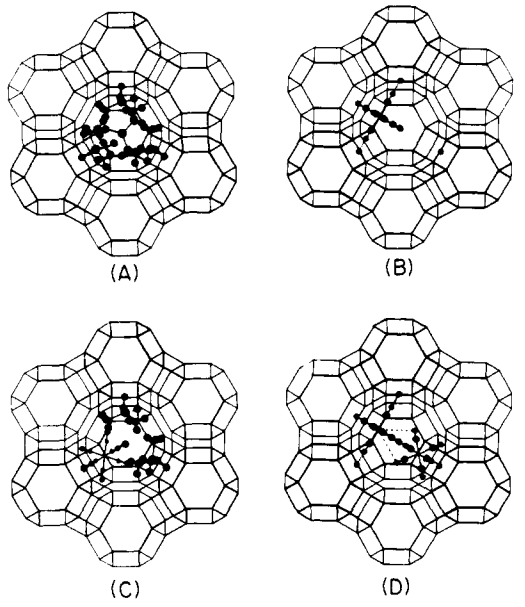

Figure 3. Molecular graphics representation of (A) 32{PMe_3}–$Na_{56}Y$; (B) 8{$Mo(CO)_6$}–$Na_{56}Y$; (C) 8{$Mo(CO)_6$}, 16{PMe_3}–$Na_{56}Y$; and (D) 16{$Mo(CO)_6$}–$Na_{56}Y$ (Chem-X Graphics).

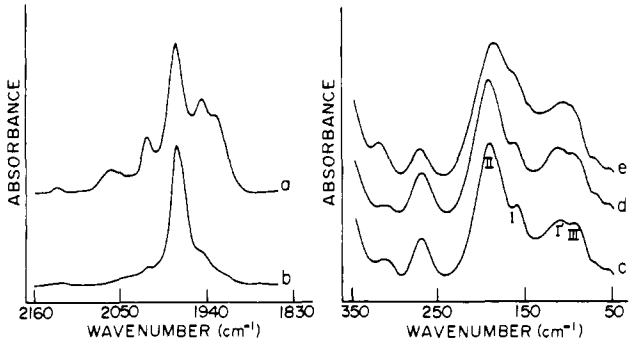

Figure 4. Mid-IR spectra of (a) annealed 4{$Mo(^{12}CO)_6$}–$Na_{56}Y$ and (b) 4{$Mo(^{12}CO)_6$},16{PMe_3}–$Na_{56}Y$. Far-IR spectra of (c) dehydrated $Na_{56}Y$; (d) annealed 4{$Mo(^{12}CO)_6$}–$Na_{56}Y$; and (e) 4{$Mo(^{12}CO)_6$},16{PMe_3}–$Na_{56}Y$.

fectly locked between two adjacent site II Na^+ ions. The interaction space offered by these Na^+ ions appears to be optimal for trapping $Mo(CO)_6$, as can be nicely judged from Chem-X space-filling models of this system, Figure 3B.

Cooperative Effects in the Nanoreactors of $Na_{56}Y$. The ν_{CO} spectral region of well-annealed n{$Mo(CO)_6$}–$Na_{56}Y$ ($0 < n \leq 8$) displays a well-resolved six-line diagnostic pattern of C_{2v} (or lower) symmetry *trans*-ZONa···(OC)$Mo(CO)_4$(CO)···NaOZ, in which the $Mo(CO)_6$ guest is optimally locked into place between two adjacent supercage site II Na^+ cations. The addition of either PMe_3 (see Chem-X space-filling model in Figure 3C) or ^{12}CO to these samples induces a partial collapse of the six-line ν_{CO} spectrum, as illustrated in Figure 4. The resulting ν_{CO} spectrum is characteristic of $Mo(CO)_6$ molecules that are more weakly anchored to two Na^+ ions.

The cation translatory modes of Na^+ found in the far-IR spectra show small but reproducible frequency shifts and intensity changes following occlusion of $Mo(CO)_6$, annealing, and addition of PMe_3, although they are much less striking than those seen in the mid-IR. The virgin dehydrated $Na_{56}Y$ shows bands at 95, 112, 162, and 192 cm^{-1} corresponding to Na^+ sites III, I', I, and II, respectively.[22] The interaction of site II Na^+ ions with $Mo(CO)_6$ shifts the corresponding band by about 1 cm^{-1}. The site III Na^+ band also shifts by about the same amount. The introduction of PMe_3 causes the site II band to shift to 187 cm^{-1}, the change of 5 cm^{-1} causing overlap with the site I Na^+ band (Figure 4). The band corresponding to site III Na^+ ions also shifts, causing overlap with the site I' Na^+ band at around 106 cm^{-1}.

The PMe_3 effect seems to be best interpreted in terms of a type of deannealing process of the $Mo(CO)_6$ guest induced by α-cage $ZONa^+$···PMe_3 interactions. These cooperative effects appear to exist between anchored $Mo(CO)_6$ guests and PMe_3 or CO ligands, as well as the cations and oxygen framework atoms of the zeolite. Strong evidence for this proposal can be found in the ^{23}Na DOR-MAS-NMR spectra of 8{$Mo(CO)_6$}–$Na_{56}Y$ before and after annealing and on subsequently saturating this sample with PMe_3 to yield the reactant pair 8{$Mo(CO)_6$},16{PMe_3}–$Na_{56}Y$. ^{23}Na ($I = {}^3/_2$, 100%) is a quadrupolar nucleus, and it can therefore interact with both magnetic fields and electric field gradients (EFGs) to yield higher order, orientation-dependent broadening that neither magic angle spinning (MAS-NMR) nor multiple pulse sequences can remove by themselves. By contrast, double rotation (DOR-NMR) averages out both first- and second-order anisotropic interactions, thereby permitting unprecedented detail to be obtained about the local environment of quadrupolar nuclei in solids.[11,13] Therefore the $Na_{56}Y$ virgin host, the 8{$Mo(CO)_6$}–$Na_{56}Y$ precursor, and the 8{$Mo(CO)_6$},16{PMe_3}–$Na_{56}Y$ reactant pair present an ideal opportunity to evaluate the usefulness of ^{23}Na DOR-NMR spectroscopy for studying anchoring interactions between the extraframework Na^+ ions and encapsulated guest, and annealing and cooperative effects.[25] Let us first focus attention on the ^{23}Na MAS-NMR spectrum[24] of fully dehydrated $Na_{56}Y$ (XRD/ND-determined site distribution:[20] I (7.1–7.7), I' (13.4–18.6), II (29.4–32.0), III (0–6.5)). Here one observes a single broad asymmetrical resonance centered around −12 ppm. In striking contrast, the ^{23}Na DOR-NMR spectrum of this same material, Figure 5a, vividly reveals that this signal in fact originates from a convolution of distinct Na^+ ion site resonances, which are assigned I (−4 ppm; double six-ring, hexagonal prism), II (−29 ppm; six-ring, α-cage) and I' (−40 ppm, six-ring, β-cage). These resonances have been identified through a combination of site-selective Na^+ ion exchanges (e.g., $Na_{56-n}Tl_nY$) and site-selective adsorption (e.g., n{$M(CO)_6$}–$Na_{56}Y$), as is described elsewhere.[25] The very low intensity of the most populous Na^+_{II} at −29 ppm in Figure 5a is at first rather surprising. The dominant effect of anchoring $Mo(CO)_6$ guests in the α-cage of $Na_{56}Y$ is always seen as a dramatic enhancement of the intensity of the −29 ppm resonance, as in Figure 5b. The relatively small intensity of the ^{23}Na DOR resonance from site II Na^+ in the virgin dehydrated $Na_{56}Y$ at around −29 ppm might originate from a distribution of chemical environments of Na^+ at this site, which could also explain the broad background ^{23}Na signal. This distribution might be brought about through motion, on the time scale of the NMR experiment, of the site II Na^+ cations between accessible sites in the spacious α-cage. However, a more ordered array of "anchored" site II Na^+ cations is formed upon adsorption of $Mo(CO)_6$ into the α-cages of $Na_{56}Y$, thus restricting the Na^+ to a specific location, with the concomitant emergence of the narrower resonance at around −24 ppm. Here one essentially "discovers" site II Na^+ by transforming "half-naked" $ZONa_{II}$ to coordinated *trans*-$ZONa_{II}$···(OC)$Mo(CO)_4$(CO)···$Na_{II}OZ$. The effect of increasing the loading of $Mo(CO)_6$ in $Na_{56}Y$ is seen to be a monotonic growth in the intensity of the Na_{II}^+ resonance with an accompanying deshielding effect of about 5 ppm at half-loading ($n = 8$). Interestingly, this deshielding of Na_{II}^+ with increasing guest loading alerts one to the existence of negative cooperativity effects, where guest–zeolite and guest–guest interactions reduce the strength of bonding between the Na_{II}^+ ions and the six-ring oxygens on the one hand, and/or the Na^+_{II} ions and the ligating oxygens of the $Mo(CO)_6$ guest on the other. Cooperative effects of this type have been observed in the loading-dependent isosteric heats of adsorption of CH_4 in NaZSM-5[26] and the loading-dependent ZONa···C_6H_6 bond distances in n{C_6H_6}–$Na_{56}Y$.[20]

A further change in the environments of the extraframework Na^+ cations is detected in the ^{23}Na DOR spectrum of the intrazeolite reactant pair, 8{$Mo(CO)_6$},16{PMe_3}–$Na_{56}Y$, Figure 5c. Here, the addition of two PMe_3 guest molecules into an α-cage containing one $Mo(CO)_6$ reactant molecule causes a downfield shift of the ^{23}Na signals associated with Na^+ at sites II and I'.

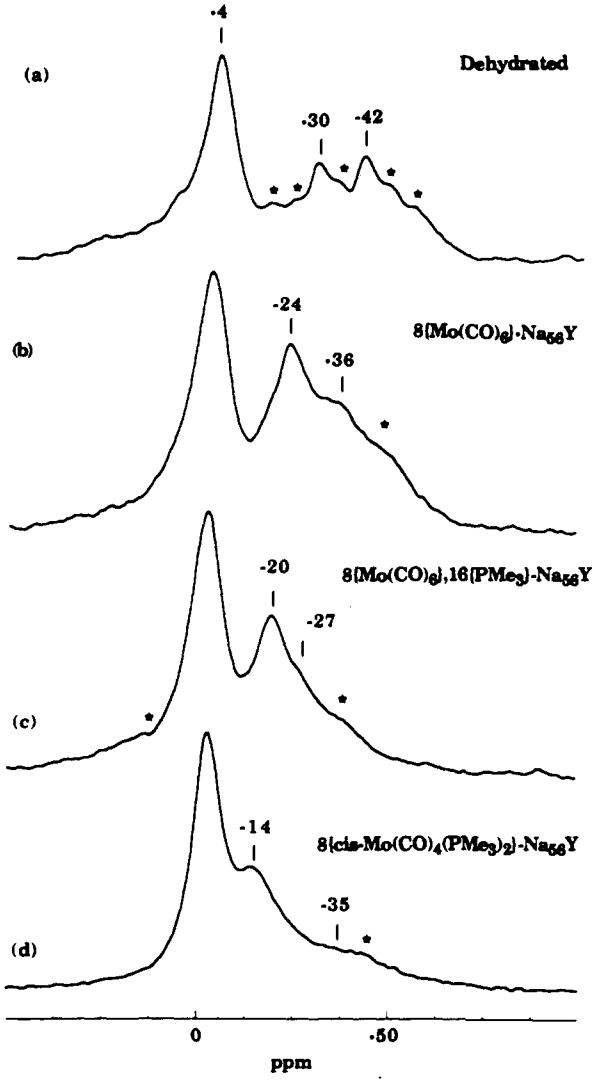

Figure 5. ^{23}Na DOR-NMR spectra of (a) dehydrated $Na_{56}Y$; (b) annealed $8\{Mo(^{12}CO)_6\}$-$Na_{56}Y$; (c) annealed $8\{Mo(^{12}CO)_6\},16(PMe_3)$-$Na_{56}Y$; and (d) annealed $8\{cis\text{-}Mo(^{12}CO)_4(PMe_3)_2\}$-$Na_{56}Y$. The asterisks denote spinning side bands.

The positions of these two resonances in the spectrum of $8\{Mo(CO)_6\},16\{PMe_3\}$-$Na_{56}Y$ are shifted significantly downfield to −20 and −27 ppm, respectively, from those of both the dehydrated $Na_{56}Y$ sample, Figure 5a, and the reactant $8\{Mo(CO)_6\}$-$Na_{56}Y$, Figure 5b. The results provide compelling evidence for a direct electronic effect exerted by the PMe_3 guests on the site II Na^+ cations anchored to the reactant $Mo(CO)_6$. The ^{23}Na DOR spectrum shown in Figure 5c also signals an indirect negative cooperative effect exerted by the PMe_3 guests on the site I′ Na^+ cations inside the adjacent sodalite cages. Additional details are to be found elsewhere.[25] This brings consistency to the conclusions drawn from mid-IR, far-IR, and DOR-NMR spectroscopy.

Identification of the Kinetic Product, $\{cis\text{-}Mo(CO)_4(PMe_3)_2\}$-$Na_{56}Y$, of the Reaction of $\{Mo(CO)_6\}$-$Na_{56}Y$ with PMe_3: Chemical, Vibrational, NMR, and EXAFS Probes. A collection of chemical and spectroscopic methods have been employed in order to unequivocally identify the product of the intrazeolite reaction of $\{Mo(CO)_6\}$-$Na_{56}Y$ with PMe_3 as $\{cis\text{-}Mo(CO)_4(PMe_3)_2\}$-$Na_{56}Y$. Thus:

(i) Using bulk $cis\text{-}Mo(CO)_4(PMe_3)_2$ and $Mo(CO)_4(DMPE)$ as SEM-EDX calibration standards, one finds that the Mo:P ratio in the kinetic product is close to 1:2.

(ii) The ν_{CO} mid-IR spectrum of the kinetic product is very similar to that of $cis\text{-}Mo(CO)_4(PMe_3)_2$ dissolved in tetrachloroethylene solution (Figure 6) but with 14–38-cm^{-1} cation-induced red frequency shifts on each of the four expected ν_{CO} modes. Thus, the ν_{CO} frequencies for $cis\text{-}Mo(CO)_4(PMe_3)_2$ in solution are 2015, 1914, 1892, and 1882 cm^{-1}, while those for $\{cis\text{-}Mo(CO)_4(PMe_3)_2\}$-$Na_{56}Y$ are 1997, 1900, 1864, and 1844 cm^{-1}.

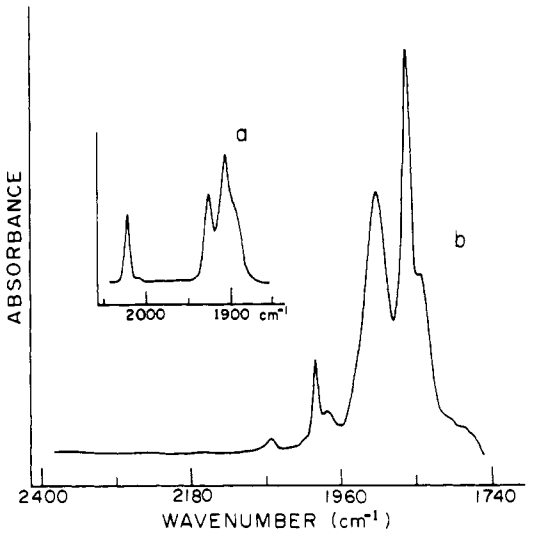

Figure 6. Mid-IR spectra of $cis\text{-}Mo(^{12}CO)_4(PMe_3)_2$ (a) in tetrachloroethylene solution and (b) occluded in $Na_{56}Y$.

These observations imply that the anchoring sites for the precursor $trans\text{-}ZONa_{11}\cdots(OC)Mo(CO)_4(CO)\cdots Na_{11}OZ$ and the kinetic product are very similar, namely, $trans\text{-}ZONa_{11}\cdots(OC)\text{-}Mo(CO)_2(cis\text{-}PMe_3)_2(CO)\cdots Na_{11}OZ$ for the latter.

(iii) The ^{31}P MAS-NMR spectrum of the kinetic product resembles the ^{31}P NMR spectrum of $cis\text{-}Mo(CO)_4(PMe_3)_2$ dissolved in benzene, except for an upfield shift of about 5.6 ppm due to the $ZONa_{11}\cdots OC$ anchoring interactions described above. Thus, the ^{31}P NMR chemical shifts, relative to 85% H_3PO_4, are −20.1 ppm for the product in $Na_{56}Y$ and −14.5 ppm for $cis\text{-}Mo(CO)_4(PMe_3)_2$ in benzene. These compare with shifts of −59.4 and −19.8 ppm for PMe_3 and $Mo(CO)_5(PMe_3)$, respectively, in $Na_{56}Y$, and with shifts of −61.0 and −17.3 ppm, respectively, in benzene.

(iv) The reaction of $\{Mo(CO)_5(PMe_3)\}$-$Na_{56}Y$ with PMe_3 yields a product identical with that from $\{Mo(CO)_6\}$-$Na_{56}Y$.[8a]

(v) The reaction of $\{Mo(CO)_6\}$-$Na_{56}Y$ with 1,2-bis(dimethylphosphino)ethane, DMPE, yields the same type of intrazeolite complex, namely, $\{cis\text{-}Mo(CO)_4(DMPE)\}$-$Na_{56}Y$, with a diagnostic mid-IR spectral pattern very similar to that of $\{cis\text{-}Mo(CO)_4(PMe_3)_2\}$-$Na_{56}Y$.

(vi) The results of EXAFS measurements have reinforced the conclusion, drawn from the above methods, that the kinetic product at low reactant loadings is indeed $\{cis\text{-}Mo(CO)_4(PMe_3)_2\}$-$Na_{56}Y$. The following is a synopsis of the Mo K-edge EXAFS structure analysis results for the kinetic product, which are presented in detail in a separate publication for the entire alkali metal cation zeolite Y series.[27] In brief, a qualitative assessment of the Fourier transforms depicted in Figure 7a,b indicates a striking similarity between the zeolite-encapsulated kinetic product and the bulk compound $cis\text{-}Mo(CO)_4(PMe_3)_2$. The plot (Figure 7c) of the Fourier filtered, inverse-transformed EXAFS data contains contributions from Mo–*C*–O, Mo–*P*, and Mo–C–*O* back-scattering for the kinetic product. Along with this, the dashed curve in Figure 7c represents the least squares fit to the standard radially symmetrical Mo K-edge EXAFS equation. The resulting parameters are shown in Table I. A comparison of the two curves in Figure 7c indicates the quality of fit, where the residual sum of squares error value was typically 6×10^{-3}.

Collected together, the above information provides compelling evidence that the kinetic product of the reaction of $\{Mo(CO)_6\}$-$Na_{56}Y$ with PMe_3 at low reactant loadings and in the absence of an externally applied pressure of CO is indeed $\{cis\text{-}Mo(CO)_4(PMe_3)_2\}$-$Na_{56}Y$.

The question of whether the $cis\text{-}Mo(CO)_4(PMe_3)_2$ is produced by the initial formation of $Mo(CO)_5(PMe_3)$, followed by a much more rapid step to form the bis-substituted product, was inves-

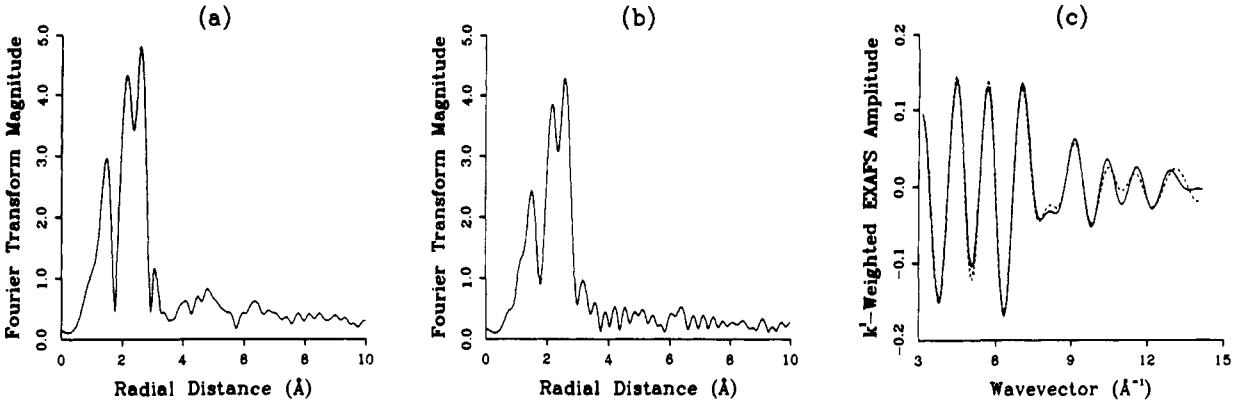

Figure 7. Fourier transform magnitudes of the base-line-corrected, normalized, k^1-weighted EXAFS data for (a) bulk *cis*-$Mo(CO)_4(PMe_3)_2$ and (b) $\{Mo(CO)_4(PMe_3)_2\}$-$Na_{56}Y$. (c) The amplitude of the EXAFS $k_1\chi$ function for the $\{Mo(CO)_4(PMe_3)_2\}$-$Na_{56}Y$ sample (solid curve) and the least squares fit obtained using amplitude and phase functions extracted from the reference compounds $Mo(CO)_6$ and *trans*-$Mo(N_2)_2(PPh_2Me)_4$ (dashed curve).

Table I. EXAFS Structural Analysis of the $\{cis\text{-}Mo(CO)_4(PMe_3)_2\}$-$Na_{56}Y$ Kinetic Product[a]

sample	atom pair[b]	coord no.	bond dist (Å)	static disorder (Å)	inner potntl (eV)
cis-$Mo(CO)_4$-$(PMe_3)_2$	Mo–*C*–O	4.00	2.04	−0.0001	−2.6
	Mo–*P*–CH_3	2.17	2.56	0.0005	1.0
	Mo–C–*O*	4.00	3.16	−0.0019	1.2
$\{cis\text{-}Mo(CO)_4$-$(PMe_3)_2\}$-$Na_{56}Y$	Mo–*C*–O	3.79	2.02	0.0000	−3.0
	Mo–*P*–CH_3	1.59	2.57	−0.0016	1.4
	Mo–C–*O*	3.79	3.16	−0.0014	−0.1

[a] Reference compounds: $Mo(CO)_6$, *trans*-$Mo(N_2)_2(PPh_2Me)_4$, and *cis*-$Mo(CO)_4(PMe_3)_2$. [b] Refers to molybdenum to italicized atom (C, P, O).

tigated by a study of the reaction of low loadings of $Mo(CO)_5(PMe_3)$ with PMe_3 at an average loading of ca. 3 molecules/α-cage. This reaction proceeded to form *cis*-$Mo(CO)_4(PMe_3)_2$, but the reaction was not quite complete after 12 h at 70 °C, whereas a reaction of $Mo(CO)_6$ with PMe_3 under similar conditions was clearly complete after only 2 h. The monosubstituted compound is therefore certainly not formed as an intermediate on the way to the *cis*-$Mo(CO)_4(PMe_3)_2$ product under these conditions. The nature of the products found under some other conditions will be described and discussed later.

Identification of the Products of the Reaction of $Mo(^{12}CO)_6$ with ^{13}CO: Mixed Isotopic Species $Mo(^{12}CO)_{6-p}(^{13}CO)_p$-$Na_{56}Y$. Determining whether or not mixed isotopic species exist in this system turns out to be a pivotal point in elucidating intimate mechanistic details of the intrazeolite reaction of $Mo(^{12}CO)_6$-$Na_{56}Y$. Under normal conditions in a kinetics run, one would have an "effective" ^{12}CO:^{13}CO ratio of ca. 1:10[3] (0.1–0.2 $Mo(^{12}CO)_6/\alpha$-cage, $P(^{13}CO)$ = 50 Torr, V = 0.75 L, assuming all ^{12}CO contained in $Mo(^{12}CO)_6$ is made available for reaction). Hence the detection of any mixed isotopic species $\{Mo(^{12}CO)_{6-p}(^{13}CO)_p\}$-$Na_{56}Y$ (p = 1–5), especially in the mid-IR spectral region of intense asymmetric ν_{CO} modes, is likely to meet with failure. To optimize the chances of detecting mixed isotopic species, the experiment must be performed under high loading conditions (1 $Mo(^{12}CO)_6/\alpha$-cage, $P(^{13}CO)$ = 50 Torr, V = 0.75 L) where the "effective" ^{12}CO:^{13}CO ratio is ca. 1:10[2], the spectra being measured in that region of the mid-IR which minimizes band overlap, i.e., the symmetric ν_{CO} modes around 2100 cm^{-1}.

Thus, the progress of the ν_{CO} band around 2100 cm^{-1} in the ^{13}CO exchange reaction of $Mo(^{12}CO)_6$-$Na_{56}Y$ (Figure 8a) shows that, at the end of a run, the spectrum is transformed into one showing a ν_{CO} band at 2073 cm^{-1} (the region of $Mo(^{13}CO)_6$-$Na_{56}Y$ absorption) with a noticeable high-frequency shoulder around 2094 cm^{-1} (Figure 8b). On evacuating this sample and adding fresh ^{13}CO, the main ν_{CO} band around 2073 cm^{-1} narrows a little and red shifts slightly to 2067 cm^{-1}. Concomitantly the intensity of the high-frequency shoulder decreases almost to 0 (Figure 8c).

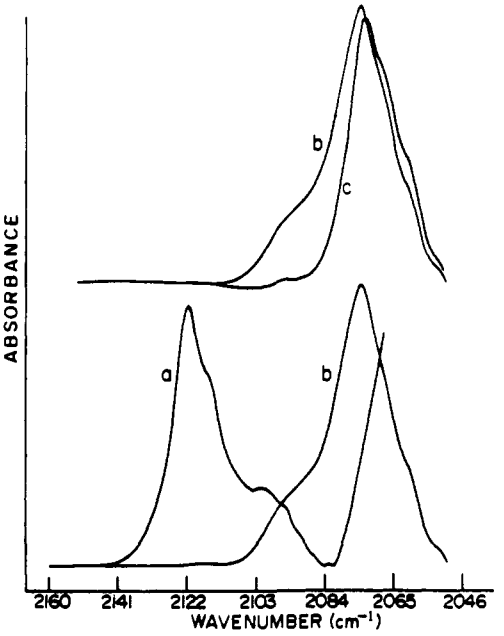

Figure 8. Symmetric stretching mid-IR region of $8\{Mo(^{12}CO)_6\}$,*m*-$\{^{13}CO\}$-$Na_{56}Y$, under 50 Torr of ^{13}CO: (a) $8\{Mo(^{12}CO)_6\}$-$Na_{56}Y$, (b) $\{Mo(^{13}CO)_6\}$-$Na_{56}Y$ and $\{Mo(^{12}CO)_{6-p}(^{13}CO)_p\}$-$Na_{56}Y$, and (c) $8\{Mo(^{13}CO)_6\}$-$Na_{56}Y$ obtained after the ^{13}CO in the cell atmosphere was renewed and the reaction was allowed to go to completion.

These experiments with high initial loading of $Mo(^{12}CO)_6$ provide unequivocal proof for the formation of mixed isotopic $\{Mo(^{12}CO)_{6-p}(^{13}CO)_p\}$-$Na_{56}Y$ species in the ^{13}CO exchange reaction of $\{Mo(^{12}CO)_6\}$-$Na_{56}Y$. Isotopomers are just observable at ^{12}CO:^{13}CO = 1:100. It is not suprising that they could be missed entirely under the normal operating conditions of a kinetics experiment where ^{12}CO:^{13}CO = ca. 1:1000, especially when it is noted that for the highest frequency, A_1, equatorial ν_{CO} stretching mode of the C_{2v} *trans*-ZONa···(OC)$Mo(CO)_4$(CO)···NaOZ species, one predicts a total of 30 mixed isotopic $Mo(^{12}CO)_{6-p}(^{13}CO)_p$-$Na_{56}Y$ molecules to absorb in the mid-IR frequency range 2160–2050 cm^{-1}!

Kinetics. The rate constants were obtained from a nonlinear least squares analysis[28] of the dependences of A_1(1975 cm^{-1}) on time t, and values obtained for reactions carried out under a wide variety of conditions are collected in Tables II–VII. Values of activation parameters obtained by a least squares analysis of the dependence of ln (k/T) on $1/T$, found for some specific conditions, are given in Table VIII.

(28) Swain, C. G.; Swain, M. S.; Berg, L. F. *J. Chem. Inf. Comput. Sci.* **1980**, *20*, 47.

Table II. Kinetics Data for Reactions of $Mo(CO)_6$ with PMe_3 in $Na_{56}Y$ at 65.8 °C: Rate-Constant Dependence on PMe_3 Loading in the Presence and Absence of an Externally Applied Pressure of CO (650 Torr)

run	$[Mo(CO)_6]$, molecules/α-cage	$\overline{PMe_3}$,[a] molecules/α-cage	[Pc],[b] molecules/nr	[Pc'],[c] molecules/"empty" cage	[Pp],[d] molecules/nr	10^4k_{obsd}, s^{-1}	10^4k_{calcd}[e] s^{-1}
			No Applied Pressure of CO				
1	0.18	0.57	0.57	0.57	0	5.27	5.31
2	0.16	1.50	1.50	1.50	0	5.19	4.56
3	0.19	1.70	1.70	1.70	0	4.34	4.47
4	0.15	2.06	2.00	2.07	0	3.99	4.24
5	0.18	2.10	2.00	2.12	0	4.33	4.21
6	0.20	2.30	2.00	2.38	0	3.71	4.00
7	0.18	2.70	2.00	2.85	0	4.08	3.67
8	0.20	4.00	2.00	4.00	0.80	2.82	3.03
9	0.15	4.90	2.00	4.00	2.40	3.92	3.48
10	0.20	6.20	2.00	4.00	5.20	4.29	4.27
			Under 650 Torr of CO				
11	0.15	1.00	1.00	1.00	0	0.95	0.72
12	0.10	2.10	2.00	2.11	0	1.40	1.44
13	0.20	2.26	2.00	2.33	0	1.47	1.44
14	0.16	3.55	2.00	3.94	0	1.66	1.44
15	0.18	3.70	2.00	4.00	0.12	1.47	1.47
16	0.20	4.00	2.00	4.00	0.80	1.69	1.66
17	0.15	5.20	2.00	4.00	3.00	2.27	2.28
18	0.16	5.80	2.00	4.00	4.24	2.74	2.63
19	0.20	6.20	2.00	4.00	5.20	3.32	2.90
20	0.16	6.30	2.00	4.00	5.24	2.44	2.91

[a] Average number of PMe_3 molecules/α-cage. [b] Number of chemisorbed PMe_3 molecules/nanoreactor (nr). [c] Number of chemisorbed PMe_3 molecules/empty α-cage, i.e., α-cages *not* containing a $Mo(CO)_6$ molecule. [d] Number of physisorbed PMe_3 molecules/nr. [e] Values calculated with parameters derived in the Discussion section.

Table III. Dependence of k_{obsd} on $P(CO)$ for Reactions of $Mo(CO)_6$ with PMe_3 at 65.8 °C and at "Low" Loadings of PMe_3[a]

run	$[Mo(CO)_6]$, molecules/α-cage	$\overline{PMe_3}$, molecules/α-cage	[Pc], molecules/nr	[Pc'], molecules/"empty" cage	[Pp], molecules/nr	$P(CO)$, Torr	10^4k_{obsd}, s^{-1}	10^4k_{calcd},[b] s^{-1}
21	0.22	3.60	2.00	4.00	0.08	50	3.55	3.18
22	0.20	3.70	2.00	4.00	0.20	100	2.79	2.52
23	0.20	3.70	2.00	4.00	0.20	150	1.91	2.11
24	0.15	3.50	2.00	3.76	0	250	1.64	1.73
25	0.17	4.00	2.00	4.00	0.68	300	1.64	1.83
26	0.19	3.70	2.00	4.00	0.16	400	1.48	1.61
27	0.15	3.60	2.00	3.88	0	500	1.59	1.54
28	0.15	3.80	2.00	4.00	0.20	520	1.67	1.59
29	0.15	3.40	2.00	3.65	0	600	1.58	1.54

[a] See footnotes to Table II for definitions. $PMe_3 \leq 4$ molecules/α-cage. [b] Calculated as described in the Discussion section.

Table IV. Dependence of k_{obsd} on $P(CO)$ for Reactions with PMe_3 at 65.8 °C and at "High" Loadings of PMe_3[a]

run	$[Mo(CO)_6]$, molecules/α-cage	$\overline{PMe_3}$, molecules/α-cage	[Pp] molecules/nr	$P(CO)$, Torr	10^4k_{obsd} s^{-1}	10^4k_{calcd},[b] s^{-1}
30	0.16	6.00	4.64	50	4.32	4.11
31	0.15	6.30	5.20	100	3.39	3.84
32	0.15	6.30	5.20	150	3.39	3.42
33	0.15	6.00	4.60	200	3.19	2.99
34	0.15	6.20	5.00	250	2.80	2.83
35	0.15	6.10	4.80	300	2.60	2.74
36	0.15	6.30	5.20	350	2.53	2.63
37	0.16	6.10	4.84	400	2.13	2.46
38	0.21	6.10	5.04	450	1.90	2.45
39	0.15	6.00	4.60	500	2.06	2.29
40	0.25	6.00	5.00	550	1.98	2.37
41	0.18	6.30	5.32	600	2.34	2.43

[a] See footnotes to Table II for definitions. [Pc] = 2.00 molecules/nr and [Pc'] = 4.00 molecules/"empty" cage. [b] Calculated as described in the Discussion section.

Discussion

1. The Environments of Reactants and Products in $Na_{56}Y$. The various spectroscopic and structural techniques applied to this system show clearly that when $Mo(CO)_6$ is initially introduced into the α-cages at relatively low loading, it is present in a metastable state with some spectroscopically detectable weak anchoring to the inner surface of the cage. Annealing at 70 °C quickly leads to a more stable form in which two *trans*-carbonyl ligands are quite strongly anchored to two Na_{II}^+ ions via their O atoms, and this in turn weakens the interactions of the Na_{II}^+ ions with their six-ring framework oxygens. Introduction of chemisorbed PMe_3 ligands into the α-cages produces a pronounced weakening of this carbonyl anchoring. The same occurs under an atmosphere of ^{13}CO.

When $Mo(CO)_6$ is introduced to its maximum loading of 2 $Mo(CO)_6$/α-cage, it is not found to undergo noticeable anchoring

Table V. Dependence of k_{obsd} on $Mo(CO)_6$ Loading for Reactions with PMe_3 at 65.8 °C and in the Presence and Absence of an Externally Applied Pressure of CO (650 Torr)

run	[$Mo(CO)_6$], molecules/α-cage	$\overline{PMe_3}$, molecules/α-cage	[Pc], molecules/nr	[Pc′], molecules/"empty" cage	[Pp], molecules/nr	10^4k_{obsd}, s^{-1}	10^4k_{calcd},[b] s^{-1}
			No Applied Pressure of CO				
42	0.04	3.10	2.00	3.15	0	3.93	3.94
5	0.18	2.10	2.00	2.12	0	4.33	4.45
43	0.40	2.00	2.00	2.00	0	3.65	3.79
44	0.71	2.83	2.00	4.00	0.50	2.47	2.34
45	0.97	2.50	2.00	4.00	0.88	1.16	(1.6)
46	1.40	2.80	0 or 2.00[c]	0[d]	3.20	26.0	
			Under 650 Torr of CO				
47	0.03	2.20	2.00	2.21	0	1.21	
48	0.48	3.2	2.00	4.00	0.16	1.10	
49	0.65	2.00	2.00	2.00	0	1.48	
50	0.77	3.20	2.00	4.00	1.48	1.33	
51	1.00	3.40	2.00	0[d]	2.80	1.76	
52	1.86	3.40	0 or 2.00[c]	0[d]	6.24	3.55	

[a] See footnotes to Table II for definitions. [b] Values calculated as described in the text. [c] Nanoreactors containing 2 $Mo(CO)_6$ molecules contain no Pc molecules, and those with 1 $Mo(CO)_6$ molecule contain 2 Pc molecules. [d] No "empty" α-cages present.

Table VI. Temperature Dependence of k_{obsd} for Reactions of $Mo(CO)_6$ with PMe_3 at "Low" Loadings of PMe_3 in the Absence of an Applied Pressure of CO and at "High" Loadings of PMe_3 under an Applied Pressure of 650 Torr of CO[a]

run	T, °C	[$Mo(CO)_6$], molecules/α-cage	$\overline{PMe_3}$, molecules/α-cage	[Pc], molecules/nr	[Pc′], molecules/"empty" cage	[Pp], molecules/nr	10^4k_{obsd}, s^{-1}
				No Applied Pressure of CO			
53	46.8	0.20	2.10	2.00	2.13	0	0.831
54	54.8	0.25	3.80	2.00	4.00	0.6	1.41
55	59.2	0.20	4.00	2.00	4.00	1.2	2.00
6	65.8	0.20	2.30	2.00	2.38	0	3.71
56	74.3	0.18	3.20	2.00	3.46	0	7.68
57	80.0	0.19	3.50	2.00	3.85	0	11.5
58	84.7	0.23	3.70	2.00	4.00	0.32	12.0
				Under 650 Torr of CO			
59	54.4	0.08	6.0	2.00	4.00	4.32	1.40
60	65.8	0.10	5.5	2.00	4.00	3.40	5.33
61	74.3	0.09	5.9	2.00	4.00	4.22	11.2

[a] See footnotes to Table II for definitions.

Table VII. Values of k_{obsd} for Reactions of ^{13}CO with $Mo(^{12}CO)_6$

run	T, °C	[$Mo(^{12}CO)_6$], molecules/α-cage	$P(^{13}CO)$, Torr	10^4k_{obsd}, s^{-1}
62	65.8	0.15	25	4.61
63	65.8	0.16	50	3.91
64	65.8	0.16	70	4.26
65	65.8	0.18	100	3.96
66	65.8	0.14	150	3.67
67	65.8	0.18	200	2.47
68	65.8	0.16	308	1.40
69	65.8	0.17	400	0.93
70	65.8	0.18	500	0.57
71	55.4	0.16	100	0.91
72	75.3	0.14	100	2.55
73	84.7	0.14	100	5.29
74	94.2	0.18	100	11.2

when annealing at 70 °C is attempted, and instead it readily undergoes CO loss to form $Mo(CO)_3$ moieties strongly anchored to three framework oxygens in the α-cage surface.[15] This emphasizes the existence of strong guest–guest influences on the anchoring strength and the nature of the reactivity.

The spectroscopic changes along the series $8\{Mo(CO)_{6-p}(PMe_3)_p\}$–$Na_{56}Y$ (p = 0–2) enable one to glean a deeper appreciation of electronic and steric contributions to the anchoring energetics of the various guests in the $n\{Mo(CO)_6\}$,$m\{PMe_3\}$–$Na_{56}Y$ system. The ν_{CO} vibrational patterns and cation-induced ν_{CO} frequency shifts of this series of intrazeolite complexes all indicate anchoring interactions of the type *trans*-$ZONa_{II}\cdots(OC)Mo(CO)_{4-p}(PMe_3)_p(CO)\cdots Na_{II}OZ$. One might expect that the much stronger net electron donor character of PMe_3 relative to that of CO should cause increasing charge density to be located on the remaining CO ligands on passing from p = 0 to p = 2, and one would suspect that this would cause the anchoring interactions to increase in strength in the same order. In this context, the ^{23}Na DOR spectrum of the kinetic product $8\{cis\text{-}Mo(CO)_4(PMe_3)_2\}$–$Na_{56}Y$, Figure 5d, features a noticeable difference from those of both the $Mo(CO)_6$ alone, Figure 5b, and the reactant pair, Figure 5c. The peak at −14 ppm in Figure 5d most likely corresponds to Na^+ cations at site II in the α-cage. The site II ^{23}Na resonance

Table VIII. Activation Parameters for Reactions of $Mo(^{12}CO)_6$ with PMe_3 or ^{13}CO in the α-Cages of $Na_{56}Y$

reactant	$\Delta H^{\ddagger}$, kJ mol^{-1}	$\Delta S^{\ddagger}$, J K^{-1} mol^{-1}	log A[a]	RMSD,[b] %
^{13}CO[c]	61 ± 5	−139 ± 13	6.1 ± 0.7	15
PMe_3[d]	70 ± 4	−106 ± 11	7.7 ± 0.6	12
PMe_3[e]	100 ± 5		12.5 ± 0.8	8
PMe_3[f]	55 ± 4	−157 ± 12	5.1 ± 0.6	12
$P(n\text{-}Bu)_3$[g]	133 ± 6	28 ± 16	14.7 ± 0.8	
$P(n\text{-}Bu)_3$[h]	91 ± 5	−62 ± 14	10.0 ± 0.7	

[a] A = preexponential term in Arrhenius equation. [b] Root mean square deviation of k from k_{calcd}, expressed as a percentage. [c] $P(^{13}CO)$ = 100 Torr; $\Delta H^{\ddagger}$ and $\Delta S^{\ddagger}$ are for the CO-dissociative process. [d] Obtained by using k_{obsd} values without correction for PMe_3 loading differences; $\Delta H^{\ddagger}$ and $\Delta S^{\ddagger}$ values apply to the combination of dissociative and associative processes. [e] $\Delta H^{\ddagger}$ and log A values apply to the combination of associative reactions with Pc and Pp. The values of $\Delta S^{\ddagger}$ would have no meaning because of standard-state definition problems. [f] Obtained after k_{obsd} values were corrected for the contribution of bimolecular reactions; i.e., $\Delta H^{\ddagger}$ and $\Delta S^{\ddagger}$ apply to the CO-dissociative process. [g] For the CO-dissociative path in xylene.[29] [h] For the associative reaction with $P(n\text{-}Bu)_3$ in xylene.[29]

shifts downfield significantly, reflecting a different interaction between the encapsulated kinetic product 8{*cis*-$Mo(CO)_4(PMe_3)_2$}-$Na_{56}Y$ and the extraframework Na^+ cations in the α-cage, compared with the analogous interaction of the reactant $Mo(CO)_6$. This is consistent with the expectation that the oxygen end of the anchoring *trans*-carbonyl ligands in 8{*cis*-$Mo(CO)_4(PMe_3)_2$}-$Na_{56}Y$ will exhibit a higher Lewis basicity than that of the reactant 8{$Mo(CO)_6$}-$Na_{56}Y$ due to the substitution of two CO by two PMe_3 ligands. Further details are to be found elsewhere.[25] However, the products of the reactions with ^{13}CO are to be regarded as only weakly bound within the α-cage because of the continued deanchoring effect of the CO present.

2. The Stoichiometric Mechanisms of the Reactions. In order to understand the detailed behavior of a $Mo(CO)_6$ guest in an α-cage, or nanoreactor, nr, of the $Na_{56}Y$ zeolite, it is necessary to determine first, as with any kinetics study of reactions in homogeneous solution, the form of the dependence of the observed rate constants on the "concentrations", in this case loadings, of the various reactants that are involved. The $Mo(CO)_6$ and PMe_3 molecules are able to diffuse initially through the zeolite lattice, for otherwise high loadings of either would be impossible, but they can nevertheless be considered to exist at the time of reaction in quite well defined sites. In this case the $Mo(CO)_6$ resides in the α-cages, and the PMe_3 molecules are either chemisorbed to site II Na^+ ions in the α-cages or physisorbed, probably in the region of the 12-ring windows of the α-cages. Note that the space available within a nr already containing one $Mo(CO)_6$ molecule and two PMe_3 molecules chemisorbed to Na^+ ions is considered to be insufficient for physisorption elsewhere inside the nr. In this context, the nr is defined as an α-cage that contains at least one $Mo(CO)_6$ molecule; i.e., empty cages are not, in this sense, nr's.

The reactions are always found to show good first-order or pseudo-first-order loss of the $Mo(CO)_6$ guest, and precise rate constants, k_{obsd}, can be obtained for any given run. The reactions of $Mo(CO)_6$ with P-donor nucleophiles in homogeneous solution are known to proceed via a mixture of CO-dissociative and associative paths,[29] the relative importance of the latter depending on the basicity and size of the nucleophiles.[29,30] A CO-dissociative path is subject to retardation in the presence of added free CO, so it is reasonable to consider first the effect of externally applied pressures of CO on the rates of reactions in the zeolite of the encapsulated $Mo(CO)_6$ guest with PMe_3.

Runs 12–15 (Table II) and 21–29 (Table III) show that when the average PMe_3 loading, $\overline{PMe_3}$, is $\leq 4/\alpha$-cage, the rates of reaction are reduced by increasing pressures of CO, but that a lower limit is approached at high $P(CO)$. When $P(CO) \geq 400$ Torr, the average value of k_{obsd} is $(1.54 \pm 0.02) \times 10^{-4}$ s^{-1}, the probable error of a single measurement being ±6.4%. Runs 18–20 (Table II) and 30–41 (Table IV) show that a similar decrease in the rates is brought about, by increasing pressures of CO, when $\overline{PMe_3}$ is ca. $6/\alpha$-cage. The lower limit in this case, estimated from the average of the values of k_{obsd} for $P(CO) \geq 400$ Torr, is $(2.36 \pm 0.17) \times 10^{-4}$ s^{-1}, but the data are more scattered, the probable error of each measurement being ±20%.

These results show that at least two reaction paths are available, one that is retarded by CO and that must involve rate-determining CO dissociation, and one or more others that are not affected by CO and that proceed at higher rates in the presence of higher loadings of PMe_3. The latter shows the importance of analyzing the effects of changes in the loading of PMe_3.

2.1 The Effect of PMe_3 Loading on Reactions with PMe_3. The effects of PMe_3 loading on the rates of reactions in the absence of an externally applied pressure of CO, or under a pressure of 650 Torr of CO, and at low and quite constant loadings of $Mo(CO)_6$, are shown by runs 1–20 in Table II. In order to analyze the effects of the various amounts of PMe_3 present in the zeolite host, it is necessary to evaluate the numbers of PMe_3 molecules present in each of the various possible environments. This can easily be done if the simplifying assumption is initially made that the distribution of the PMe_3 molecules is homogeneous and not statistical; e.g., at an average loading of 2 PMe_3 molecules/α-cage, assume that there really are 2 PMe_3 molecules in each α-cage and that they are not distributed with some cavities having 0, 1, 3, and 4 PMe_3 molecules in them. The kinetics results will be seen to be consistent with this hypothesis. A homogeneous distribution of the $Mo(CO)_6$ molecules can also be assumed.[18]

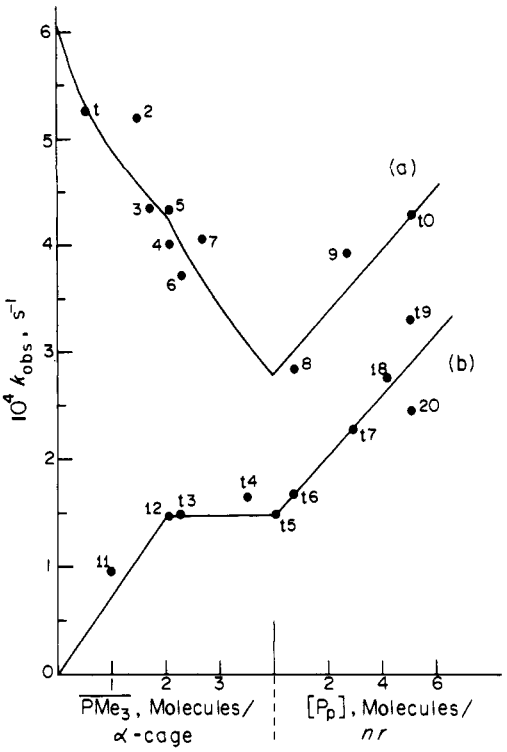

Figure 9. Dependence of k_{obsd} on PMe_3 loading at low $Mo(CO)_6$ loading (a) in the absence of any applied pressure of CO and (b) under an applied pressure of 650 Torr of CO. The numbers refer to the run numbers in Table II, and the lines drawn are the theoretical lines as derived in the text.

The calculations of the numbers of PMe_3 molecules in the various environments can therefore be carried out. For example, in run 7 there are 0.18 $Mo(CO)_6$ molecules/α-cage and an average of 2.70 PMe_3 molecules/α-cage. Each of the nr's, i.e., α-cages that are singly occupied by a $Mo(CO)_6$ molecule, can accommodate 2 PMe_3 (Pc) molecules, chemisorbed to the 2 Na^+ ions that are not potentially or actually used to anchor the $Mo(CO)_6$ molecule in the nr. This accounts for 0.36 of the 2.70 PMe_3 molecules/α-cage, leaving 2.34 PMe_3 molecules that can be distributed evenly among the 0.82 "empty" cages (i.e., those not occupied by $Mo(CO)_6$ molecules). This leads to a loading of 2.85 chemisorbed PMe_3 (Pc') molecules/empty α-cage. For run 9, with a loading of 0.15 $Mo(CO)_6$ molecules/α-cage and an average of 4.9 PMe_3 molecules/α-cage, there are 2 Pc molecules/nr (0.30 of the 4.9 PMe_3/molecules) and 4 Pc' molecules/empty α-cage (another $4 \times 0.85 = 3.4$ PMe_3 molecules), and the remaining 1.2 PMe_3 molecules/α-cage have to be physisorbed (i.e., as Pp molecules), most probably in the region of the 12-ring windows of the α-cages. Although each α-cage has four such windows, each window is shared between two α-cages so that there are only two windows per α-cage on average. A loading of 1.2 Pp molecules/α-cage means that there are 0.6 Pp molecules in each window throughout the lattice, and this in turn means that there are $4 \times 0.6 = 2.4$ Pp molecules available to each $Mo(CO)_6$ molecule in an isolated nr. It can be seen that in some cases (runs 10 and 18–20) there is more than one Pp molecule estimated to be in some of the four 12-ring windows of the nr's or otherwise weakly bound.

(29) Angelici, R. J.; Graham, J. R. *J. Am. Chem. Soc.* **1966**, *88*, 3658; *Inorg. Chem.* **1967**, *6*, 2082.
(30) Poë, A. J.; Twigg, M. V. *J. Organomet. Chem.* **1973**, *50*, C39. Brodie, N. M. J.; Chen, L.; Poë, A. J. *Int. J. Chem. Kinet.* **1988**, *20*, 467.

The data can now be represented graphically as follows. When there are ≤4 Pc′ molecules/empty α-cage, we can plot k_{obsd} against $\overline{PMe_3}$, and when $\overline{PMe_3}$ is higher, such that there are 2 Pc molecules/nr, 4 Pc′ molecules/empty cage, and some Pp molecules in the windows, we can plot k_{obsd} against [Pp], the number of Pp molecules/nr. This is done in Figure 9, and we can consider first the reactions carried out under 650 Torr of CO. The values of k_{obsd} increase from $\overline{PMe_3}$ = 1 to ca. 2 molecules/α-cage, after which they remain effectively constant up to $\overline{PMe_3}$ = 4 molecules/α-cage. When $\overline{PMe_3}$ is higher, so that all the chemisorption sites are full, then k_{obsd} increases linearly with [Pp]. Reaction with Pp is therefore clearly first order in $[Mo(CO)_6]$ and [Pp]. A linear least squares analysis of the dependence of k_{obsd} on [Pp] can be carried out with each value of k_{obsd} being weighted according to the assumption of a constant probable error, expressed as a percentage, for each measurement of k_{obsd}. This leads to a second-order rate constant, k_a(Pp), of $(0.26 \pm 0.05) \times 10^{-4}$ s^{-1} (molecules/nr)$^{-1}$, the probable error of each measurement of k_{obsd} being ±11.7%.

Reactions with Pc molecules can also be considered to be first order in [Pc], where [Pc] represents the number of Pc molecules *per nanoreactor*. This can be concluded because k_{obsd} does increase from $\overline{PMe_3}$ = [Pc] = 1 to 2 molecules/nr but remains constant from $\overline{PMe_3}$ = 2 to ca. 4 molecules/α-cage. Over this range [Pc], in molecules/nr, remains constant at 2, even though the number of Pc′ molecules/empty α-cage is increasing. It is therefore evident that Pc′ molecules in empty α-cages adjacent to the nr's cannot participate in the second-order reaction which occurs only with Pc molecules, i.e., PMe_3 molecules present together with $Mo(CO)_6$ in a nr. However, there could still be rapid exchange of Pc and Pc′ molecules between nr's and empty α-cages. The average value of k_{obsd} from runs 12–14 is $(1.46 \pm 0.14) \times 10^{-4}$ s^{-1}, and this is in complete agreement with the value of the intercept at [Pp] = 0 (also $(1.46 \pm 0.14) \times 10^{-4}$ s^{-1}) obtained independently from the least squares analysis of the dependence of k_{obsd} on [Pp]. A value of $(0.73 \pm 0.05) \times 10^{-4}$ s^{-1} (molecules/nr)$^{-1}$ for k_a(Pc) can therefore be obtained, taking into account the fact that there are 2 Pc molecules/nr.

The values of k_{obsd} for reactions in the absence of any applied pressure of CO decrease with increasing $\overline{PMe_3}$ up to $\overline{PMe_3}$ = 2.7 molecules/α-cage. These reactions are still presumably proceeding by the second-order process (first order in [Pc]) discussed above so that the values of k_d for the CO-dissociative path can be obtained from $k_d = k_{obsd} - k_a$(Pc)[Pc], the values of k_a(Pc)[Pc] being derivable simply from the linear plots in Figure 9 through the values of k_{obsd} for reactions under 650 Torr of CO and with $\overline{PMe_3}$ = 0–2.7 molecules/α-cage.

The values of k_d so obtained can conveniently be transformed into values of $\Delta G_d^{\ddagger}$, and these are plotted against $\overline{PMe_3}$ in Figure 10. The values of $\Delta G_d^{\ddagger}$ increase linearly with $\overline{PMe_3}$, and an unweighed least squares analysis leads to a value of $\Delta G_d^{\ddagger}(\overline{PMe_3} = 0) = 104.1 \pm 4.4$ kJ mol^{-1} and a gradient of 1.04 ± 0.23 kJ mol^{-1} (PMe_3 molecules/α-cage)$^{-1}$. The probable erorr in k_d that corresponds to the scatter around the $\Delta G_d^{\ddagger}$ vs $\overline{PMe_3}$ plot is ±9.2%, so that the fit of the data to the model must be considered to be very satisfactory. The line drawn through the values of k_{obsd} for reactions in the absence of CO and with $\overline{PMe_3}$ = 0–4 molecules/α-cage (Figure 9) corresponds to the calculated values of $k_d + k_a$(Pc)[Pc] (see below), the unusual shape resulting from the combination of the exponential decrease of k_d with increasing $\overline{PMe_3}$ and the discontinuous change of k_a(Pc) with $\overline{PMe_3}$. The calculated line has been extended to $\overline{PMe_3}$ = 4, [Pp] = 0, where the calculated value of the rate constant is found to be $(2.81 \pm 0.52) \times 10^{-4}$ s^{-1}.

At higher values of $\overline{PMe_3}$, where [Pp] becomes significant, the rates increase monotonically with [Pp], and the gradient given by a weighted linear least squares analysis is $(0.35 \pm 0.14) \times 10^{-4}$ s^{-1} (Pp molecules/nr)$^{-1}$, a value essentially indistinguishable from the value of k_a(Pp) derived above from the data under 650 Torr of CO. The RMSD of the three points from the line is ±6.7%, and the standard deviation is ±11.6%.[31] The intercept at [Pp] = 0 is $(2.69 \pm 0.35) \times 10^{-4}$ s^{-1}, which is in excellent agreement with the value calculated above from the extrapolation of the $\overline{PMe_3}$ dependence to $\overline{PMe_3}$ = 4, [Pp] = 0.

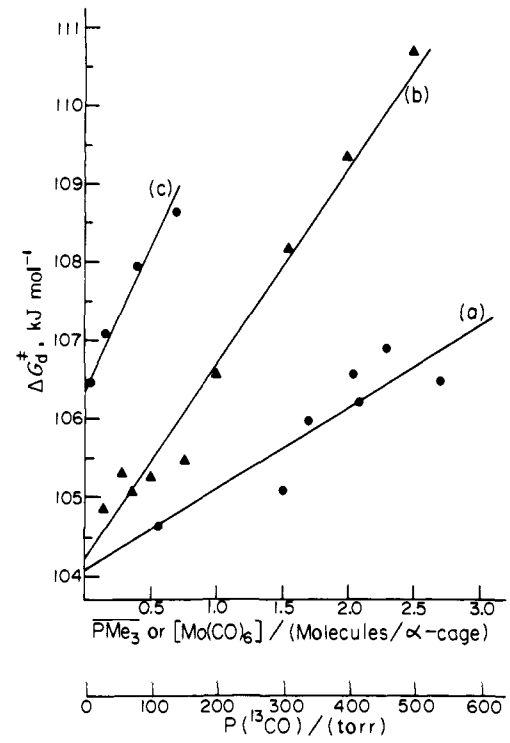

Figure 10. Plots of $\Delta G_d^{\ddagger}$ for reactions with (a) varying loadings of PMe_3, (b) varying pressures of ^{13}CO, and (c) varying loadings of $Mo(CO)_6$.

We can now calculate values (Table II) of the rate constants corresponding to all the values of k_{obsd} for runs 1–20 by using the parameters $10^4 k_d = 6.04 \exp(-0.37\overline{PMe_3})$ s^{-1} (derived from the linear dependence of $\Delta G_d^{\ddagger}$ on $\overline{PMe_3}$), $10^4 k_a$(Pc) = 0.73 s^{-1} (Pc molecules/nr)$^{-1}$, and $10^4 k_a$(Pp) = 0.27 ± 0.05 s^{-1} (Pp molecules/nr)$^{-1}$, the latter being the weighted average of the two values found either under 650 Torr of CO or in the absence of CO. The probable error of measurement of each of the 20 rate constants is then found to be ±12.2%, a very satisfactory result considering the wide variations of PMe_3 loading and P(CO) involved, and the lines drawn in Figure 9 correspond to the values of k_{calcd} given in Table II.

2.2 The Effect of P(CO) on Reactions with PMe_3. The effect of an increasing applied pressure of CO on the rates of reaction with [Pc] = 2 molecules/nr and [Pc′] ≤ 4 molecules/empty cage is shown by runs 21–29 (Table III) and 12–14 (Table II). In most cases small corrections have to be made to k_{obsd} to remove contributions to the rates due to the second-order reactions with Pp molecules. Corrections for the $\overline{PMe_3}$ dependence of those runs with [Pp] = 0 are also small, and the values of k_{cor} appropriate to $\overline{PMe_3}$ = 4 and [Pp] = 0 are plotted against P(CO) in Figure 11. The line through the data has been drawn according to eq 1, with $a = 2.2$ s^{-1}, $b = 1.2 \times 10^{-4}$ Torr^{-2}, and $c = 1.46$ s^{-1}. The

$$10^4 k_{cor} = a/\{1 + b[P(CO)]^2\} + c \qquad (1)$$

probable error of determination of each rate constant is ±9.0%, which reflects the rather small scatter of the data around the line.

(31) Where only a few points are available for a least squares analysis, it is preferable to use the smaller root mean square deviation, RMSD, rather than the standard deviations, which are high because of the small number of degrees of freedom, provided the result is not in disagreement with the values of the standard deviations derived from larger sets of data. In the case referred to in the text, the standard deviation is probably a more realistic estimate of the goodness of fit.

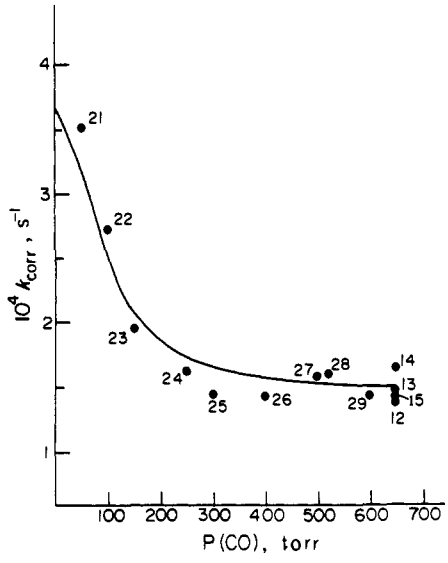

Figure 11. Dependence on $P(CO)$ of k_{cor}, i.e., k_{obsd} corrected to [Pc] = 2 molecules/nr and [Pc'] = 4 molecules/"empty" cage. The numbers refer to the run numbers listed in Tables II and III, and the line is the theoretical line drawn according to eq 1 and the parameters derived in the text.

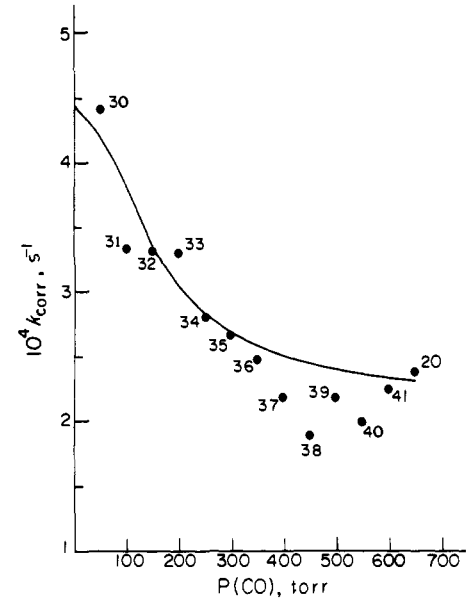

Figure 12. Dependence on $P(CO)$ of k_{cor}, i.e., k_{obsd} corrected to [Pc] = 2 molecules/nr, [Pc'] = 4 molecules/"empty" cage, and [Pp] = 5 molecules/nr. The numbers refer to the run numbers in Tables II and IV, and the line is the theoretical line drawn according to eq 1 and the parameters derived in the text.

The RMSD of the data for runs 21–24 is ±9.8%, and it is these data that do most to define the values of a and b, but the number of points available in this range of $P(CO)$ is not great enough to provide meaningful estimates of the uncertainties in a and b. The value of c is the same as that found from k_a(Pc), reflecting the fact that the dissociative reaction is essentially quenched under 650 Torr of CO, a fact supported by the value of b, which predicts that the dissociative path is retarded by over 98% under 650 Torr of CO, and by ca. 94% under 400 Torr of CO. The value of $(a + c)$ is 3.66 s^{-1}, which is somewhat higher than the value 2.81 ± 0.52 s^{-1} predicted above by the $\overline{PMe_3}$ variation but still within reasonable error limits. The general fit of the data to eq 1 and, particularly, the importance of the term $b[P(CO)]^2$, are therefore well established.

The effect of $P(CO)$ on the reactions with [Pc] = 2 molecules/nr and [Pc'] = 4 molecules/empty cage and with [Pp] = 5 molecules/nr can be determined from runs 30–41 (Table IV) and 20 (Table II) (all of which were carried out at the same time). After corrections are made for the different values of [Pp] involved, the values of k_{cor} can be plotted against $P(CO)$ as in Figure 12. The line drawn through the data corresponds to eq 1 with a = 2.2 ± 0.3 s^{-1}, b = 0.4 ± 0.1 $Torr^{-2}$, and c = 2.2 s^{-1}. The uncertainties in a and b were obtained from a linear least squares analysis of the dependence of $1/\{10^4 k_{co4} - c\}$ on $[P(CO)]^2$, and the value of c is within the error limits of the average of all the values obtained for runs with $P(CO) \geq 400$ Torr when the value of b predicts that the dissociative path is retarded by at least 90%. The value $(a + c)$ = 4.4 ± 0.3 s^{-1} agrees very well with the value 4.2 s^{-1} predicted from the parameters used above in the full analysis of runs 1–20. The general fit of the data to eq 1 is therefore very satisfactory, although some systematic errors are clearly evident at higher values of $P(CO)$ (Figure 12), the reasons for which are not yet clear.

2.3 The Effect of $Mo(CO)_6$ Loading on the Reactions with PMe_3. Runs 42–46 and 5 (Table V) provide evidence for the effect of increasing the $Mo(CO)_6$ loading from 0.04 to 1.4 molecules/α-cage in the absence of CO, and runs 12–15 (Table II) and 47–52 (Table V) provide similar evidence for the effect of increasing $Mo(CO)_6$ loading from 0.03 to 1.86 molecules/α-cage under 650 Torr of CO.

Runs 48 and 50–52 (Table V) were all performed with high enough $Mo(CO)_6$ loadings (≥0.48/α-cage) for all possible chemisorption sites to be fully occupied by either $Mo(CO)_6$ or PMe_3 molecules, and for there to be varying values of [Pp] brought about by the high and variable $Mo(CO)_6$ loadings. The data for these reactions are plotted against [Pp] on the right-hand side of Figure 13, and the line drawn is based on a weighted linear least squares analysis that leads to $k_a(Pp) = (0.34 \pm 0.07) \times 10^{-4}$ s^{-1} $(molecules/nr)^{-1}$. This value is indistinguishable from the weighted average of the two values obtained previously at much lower $Mo(CO)_6$ loadings and in the absence or presence of 650 Torr of CO.

Runs 12–14, 47, and 49 all have 2 Pc molecules/nr and no Pp molecules, and runs 15 and 48 both have 2 Pc molecules/nr and a small number of Pp molecules/nr, the effect of which on the values of k_{obsd} is small and can be allowed for by using the value of k_a(Pp). We therefore have seven values of rate constants for reactions under 650 Torr of CO and in the absence of any Pp molecules, covering a range of $Mo(CO)_6$ loading from 0.03 to 0.65 molecules/nr. These are plotted against $Mo(CO)_6$ loading on the lower left-hand side of Figure 13. There appears to be a slight decrease of k_{obsd} (corrected for k_a(Pp) where necessary) at higher $Mo(CO)_6$ loading, an interpretation that is allowed by the values at 0.48 and 0.65 $Mo(CO)_6$ molecules/α-cage and positively supported by the intercept at [Pp] = 0, $k_{obsd} = (0.95 \pm 0.14) \times 10^{-4}$ s^{-1} on the plot of k_{obsd} vs [Pp].

The values of k_{obsd} for reactions in the absence of CO show a decrease with increasing $Mo(CO)_6$ loading (runs 5 and 42–45) over the range 0.04–0.97 molecules/α-cage. In these cases corrections have to be applied to allow for the effect of different PMe_3 loadings on the dissociative path, for significant values of [Pp] for two of the runs, and for the slight and not very well defined decrease of k_a(Pc) with increasing $Mo(CO)_6$ loading indicated by the reactions under 650 Torr of CO. The resulting values appropriate to $\overline{PMe_3}$ = 3 molecules/α-cage are also plotted in Figure 13. The data from runs 5 and 42–44 lead to a linear increase of ΔG_d^* with increasing $Mo(CO)_6$ loading, as shown in Figure 10, and the least squares line drawn through these data corresponds to $\Delta G_d^* = (106.5 \pm 0.2) + (3.2 \pm 0.4)[Mo(CO)_6]$ kJ mol^{-1}, with $\sigma(k_{obsd}) = \pm 7\%$. The extrapolation of this line in Figure 10 to a loading of 0.97 molecules/α-cage predicts a considerably larger rate constant, 1.6×10^{-4} s^{-1}, than the 0.91×10^{-4} s^{-1} obtained under these conditions (i.e., run 45 corrected for the effect of the Pp present). The amount of CO released during this reaction at high $Mo(CO)_6$ loading may be sufficient to decrease the rate substantially, and other more general environmental effects of approaching a loading of 1 $Mo(CO)_6$ molecule/α-cage may also be important.

Run 46, recorded in Table V and carried out in the absence of CO, is exceptional in having 2 $Mo(CO)_6$ molecules and no Pc molecules in 40% of the nanoreactors, so reactions in these nr's involve only Pp molecules. The rate is very greatly increased as a result, and to a much greater extent that could be explained by the value of $k_a(Pp)[Pp]$.

2.4 The Kinetics of the CO-Exchange Reaction. The values of k_{obsd} for reactions of $Mo(^{12}CO)_6$ with ^{13}CO show a simple exponential decrease with increasing $P(^{13}CO)$ up to 500 Torr.[32] No significant lower limit is observable, as shown by the good linearity of a plot of ln k vs $P(^{13}CO)$ and also by the closely linear increase of $\Delta G^{\ddagger}$ with $P(CO)$ shown in Figure 10. This reaction must therefore be proceeding only by the dissociative process. The scatter around this line leads to $\sigma(k_{obsd}) = \pm 12.9\%$, and the gradient is 1.27 ± 0.07 kJ mol^{-1} (100 Torr)$^{-1}$. The intercept at $P(^{13}CO) = 0$ is 104.4 ± 0.2 kJ mol^{-1}, which is identical with the value of $\Delta G_d^{\ddagger}(\overline{PMe_3} = 0)$ for the dissociative reaction with PMe_3.

2.5 The Temperature Dependence of the Reactions. The temperature dependence of the dissociative CO exchange reaction under 100 Torr of ^{13}CO (a pressure appropriate to that part of the cell (Figure 1) exposed to ambient temperature and presumably characteristic also of the pressure in the nr's) was investigated at quite constant $Mo(CO)_6$ loading (Table VII), and the analysis is quite unambiguous. The data give a reasonable fit to the Eyring equation, provided that one obviously deviant point is omitted, and the activation parameters are given in Table VIII.

The temperature dependence of the reactions with PMe_3 has been studied under two quite different sets of conditions. Runs 53–58 (Table VI) were performed in the absence of an applied pressure of CO with an almost constant loading of $Mo(CO)_6$ and with $\overline{PMe_3} = 2$–4 molecules/α-cage. The latter results in there being 2 Pc molecules/nr, 2–4 Pc′ molecules/empty cage, and in three runs, some small amounts of Pp. The variation in $\overline{PMe_3}$ would lead to a variation of no more than ±20% in k_{obsd} at 65.8 °C (Figure 9), and the variation in [Pp] would have a much smaller effect. The values of k_{obsd}, unadjusted for any effects of different PMe_3 loadings, give quite a good fit to the Eyring equation with a rough inverse correlation of the deviations with $\overline{PMe_3}$; i.e., high positive values of the deviations are associated with low $\overline{PMe_3}$, and vice versa, as expected. The activation parameters are given in Table VIII and apply to k_{obsd} values that measure the *sum* of the rate constants for the dissociative and associative paths (with Pc) in roughly equal proportions. Corrections for variations of PMe_3, and for the presence of Pp, required the assumption of similar proportional changes of the rates with $\overline{PMe_3}$ and [Pp] at each temperature. When such corrections were applied, no significant changes in the activation parameters were obtained, but the fit was not as good, presumably because some of the corrections were too large and the assumptions on which they were based were questionable.

Runs 59–61 (Table VI) involved associative reactions under 650 Torr of CO with constant and low $Mo(CO)_6$ loadings, maximum Pc and Pc′ loading, and [Pp] = 3.40–4.32 molecules/nr. Small corrections to [Pp] = 4.27 molecules/nr (the average value of [Pp] used) could be made by assuming a similar proportional change in k_{obsd} with [Pp] at each temperature, and the fit to the Eyring equation is then quite good; the activation parameters are given in Table VIII. These result from the temperature dependence of the sum $2k_a(Pc) + 4.27k_a(Pp)$. Although the value of $\Delta H_a^{\ddagger}$ so obtained will have some significance for comparative purposes, the value of $\Delta S_a^{\ddagger}$ will be virtually meaningless because of the essentially undefinable standard state for the combination of Pc and Pp nucleophiles and the absence of clearly defined units. On the other hand, values of the Arrhenius preexponential term, A, do have precisely defined units of s^{-1} and represent reaction probabilities under the defined conditions, and the log A value is given instead of $\Delta S_a^{\ddagger}$ in Table VIII.

Now that we know the temperature dependence of $k_{obsd} = 2k_a(Pc) + 4.27k_a(Pp)$, it is possible to obtain rough estimates of the activation parameters for the reaction with PMe_3 by the dissociative path alone. We have to make the approximate assumption that the proportion of the associative reactions that occur with Pc molecules remains constant with temperature, so that calculated values of $k_a(Pc)$ for runs 53–58 can be obtained and used to obtain k_d from k_{obsd}. Corrections to $\overline{PMe_3} = 3/\alpha$-cage can also be made as described above, but corrections for different [Pp] values turn out to be too large, and the data for runs 54, 55, and 58 have to be ignored. The values of $\Delta H_d^{\ddagger}$ and $\Delta S_d^{\ddagger}$ so obtained are given in Table VIII. The parameters are indistinguishable from those obtained directly from reactions with ^{13}CO without the need for any corrections. The fact that a higher value of $\Delta H^{\ddagger}$ is obtained when corrections for the associative path are not made results from the higher value of $\Delta H_a^{\ddagger}$ compared to $\Delta H_d^{\ddagger}$ (Table VIII).

2.6 Summary of the Stoichiometric Mechanisms. The stoichiometric mechanisms of the reactions of $Mo(CO)_6$ in the α-cage of sodium zeolite Y with PMe_3 and ^{13}CO are clearly established by the analysis of the data presented above. The fit of the data to the proposed rate equations is generally very good, with probable errors of k_{obsd} values usually being close to ±10%, but systematic errors do occasionally occur for reasons that are not obvious.

Reactions with PMe_3 are inhibited by CO in accordance with the sequence of reactions shown in eqs 2–5, for which the rate eqs 6 and 7 can be derived:

$$Mo(CO)_6 \underset{k_{-1}}{\overset{k_1}{\rightleftharpoons}} Mo(CO)_5 + CO \quad (2)$$

$$Mo(CO)_5 \underset{k_{-2}}{\overset{k_2}{\rightleftharpoons}} Mo(CO)_4 + CO \quad (3)$$

$$Mo(CO)_4 + L \xrightarrow{k_3} Mo(CO)_4L \quad (4)$$

$$Mo(CO)_4L + L \xrightarrow{fast} cis\text{-}Mo(CO)_4L_2 \quad (5)$$

$$k_d = k_1k_2k_3[L]/\{k_2k_3[L] + k_{-1}k_{-3}P(CO)[L] + k_{-1}k_{-2}[P(CO)]^2\} \quad (6)$$

or

$$1/k_d = 1/k_1 + k_{-1}P(CO)/k_1k_2 + k_{-1}k_{-2}[P(CO)]^2/k_1k_2k_3[L] \quad (7)$$

If $k_{-2}P(CO) \gg k_3[L]$, eq 7 transforms to eq 8,

$$1/k_d = 1/k_1 + k_{-1}k_{-2}[P(CO)]^2/k_1k_2k_3[L] \quad (8)$$

which is the same in form as the first term in eq 1, with $a = k_1$ and $b = k_{-1}k_{-2}/k_2k_3[L]$. Since there are two types of L (Pc and Pp) involved in eq 4, $k_3[L]$ should be replaced by $k_3(Pc)[Pc] + k_3(Pp)[Pp]$. It is noteworthy that, as expected, b is significantly smaller, $(0.4 \pm 0.16) \times 10^{-4}$ vs 1.2×10^{-4} Torr^{-2}, when Pp molecules are present than when they are not, the difference being large enough that the conclusion is unlikely to be affected by the lack of objective error limits for the value of b in the absence of any Pp molecules. The sequence of reactions shown in eqs 2–5 is also supported by the fact that *cis*-$Mo(CO)_4(PMe_3)_2$ is the *only* product in the absence of CO.

Reaction of $Mo(CO)_6$ with PMe_3 can also occur by processes that are not inhibited by CO. Reactions with Pp molecules are clearly first order in [Pp], and reactions with Pc are also most probably first order in [Pc], so there are two types of associative reactions depending on the type of PMe_3 nucleophiles involved.

On the other hand, the exchange reaction of $Mo(^{12}CO)_6$ with ^{13}CO does not show a path that is first order in $P(^{13}CO)$, so we conclude that only a CO-dissociative path is involved in spite of the fact that retardation by added ^{12}CO was not investigated. At low $Mo(^{12}CO)_6$ loadings, when no significant partial pressure of ^{12}CO is built up during the reactions, the product appears to be mainly the isotopomer $Mo(^{13}CO)_6$. The fact that the product is not simply *cis*-$Mo(^{12}CO)_4(^{13}CO)_2$ shows that when Mo-

(32) These data also show a good fit to eq 1 in ref 8b, but we believe that this is an algebraic coincidence. The exponential form and its consequent effect on $\Delta G_d^{\ddagger}$ are in good agreement with the effects of PMe_3 and $Mo(CO)_6$ loading changes (Figure 10) and are chemically more reasonable.

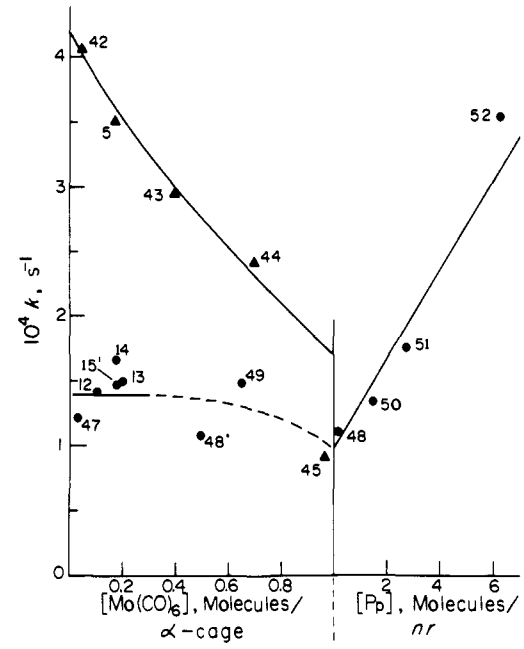

Figure 13. Dependence of k on [Pp] and $Mo(CO)_6$ loading. Points 48 and 50–52 indicate the dependence of k_{obsd} on [Pp], where the Pp molecules were generated from quite low loadings of PMe_3 by large and variable loadings of $Mo(CO)_6$. Points 5 and 42–45 represent the dependence of the rate constants at $P(CO) = 0$ for the corresponding run numbers in Table V which have been corrected to what they would have been at $\overline{PMe_3} = 3$ molecules/α-cage and [Pp] = 0. The line drawn is the theoretical line calculated as described in the text. Points 12–14, 47, and 49 show the dependence of k_{obsd} ($P(CO)$ = 650 Torr) on $Mo(CO)_6$ loading for the corresponding run numbers in Tables II and V. Points 15′ and 48′ are the rate constants (for the corresponding run numbers in Tables II and V) that have been corrected for the small contributions of k_a(Pp).

($^{12}CO)_4(^{13}CO)$ is formed by reaction 4 (L = ^{13}CO), the latter loses ^{12}CO (with a first-order rate constant of $(4/5)k_2$, where the factor $^4/_5$ represents the statistical factor for loss of ^{12}CO) to form $Mo(^{12}CO)_3(^{13}CO)$ rather than adding another ^{13}CO by a second-order process as in reaction 5 (L = ^{13}CO), which is effectively irreversible under these conditions. This process of rapid $^{12}CO/^{13}CO$ exchange in $Mo(CO)_4$ must continue until $Mo(^{13}CO)_4$ is formed virtually pure, after which reactions 4 and 5 (L = ^{13}CO) produce the equally pure product $Mo(^{13}CO)_6$. However, when the 10×-higher loading of $Mo(^{12}CO)_6$ is used, a 10×-larger partial pressure of ^{12}CO is built up during the reaction. This will affect the distribution of isotopomers $Mo(^{12}CO)_{4-p}(^{13}CO)_p$ during the $^{12}CO/^{13}CO$ exchange process in favor of the less completely substituted forms, and it will also enhance the probability that $Mo(^{12}CO)_{5-p}(^{13}CO)_p$ will be formed from them and that the latter will react with ^{12}CO. The probability that mixed $Mo(^{12}CO)_{6-p}(^{13}CO)_p$ products will be formed will consequently be greater, as observed (Figure 8b).

3. The Intimate Mechanisms. 3.1. The Activation Parameters. The reactions of $Mo(CO)_6$ in the α-cages of sodium zeolite Y at 65.8 °C are ca. 10^3 times faster than corresponding reactions in homogeneous solution after correction for the temperature dependence of the latter.[29] In the case of the dissociative path this is brought about by a major decrease in $\Delta H_d^{\ddagger}$, which is offset to a large extent by a much more unfavorable value of $\Delta S_d^{\ddagger}$. These changes can be accounted for by a substantial increase in the extent of anchoring of the $\{Mo(CO)_5\cdots CO\}^{\ddagger}$ transition state compared to that of the weakly anchored ground state $Mo(CO)_6$ molecule itself. It has been clearly demonstrated that the anchoring of the $Mo(CO)_6$ molecule by the two Na_{II}^+ ions to which it is attached when alone in the α-cage is greatly weakened by the introduction of either PMe_3 or CO molecules. As one CO molecule begins to dissociate from the $Mo(CO)_6$ molecule, the remaining CO ligands will each have a greater share of the six d_π electrons that are available for back-donation. This effect may be concentrated in two CO ligands trans to each other and close to two Na_{II}^+ ions so that the extra negative charge built up on these O atoms will develop a much stronger anchoring to the Na_{II}^+ ions.

This effect will be enhanced by another phenomenon that is likely to occur. It is known that carbonyls such as $Mo(CO)_6$ can react thermally in the α-cages, in the absence of added reagents, to lose three CO ligands and form a product in which the three coordination sites thus made available are occupied by three framework oxygens of the six-rings acting as a chelating zeolate ligand.[15,33] It seems highly probable that this process can begin during the loss of the first CO ligand so that the CO is progressively replaced by a developing ZO···$Mo(CO)_5$ bond. Since the framework oxygens are probably good donors compared with the departing CO ligand, this will greatly increase the capacity of the Mo atom to donate π–electrons to the remaining CO ligands, which become much more strongly anchored as a result.

These interactions in the transition state will require rather precise, "lock and key" positioning of the atoms involved, particularly as compared to the relatively much freer $Mo(CO)_6$ molecule in its ground state, and this can account for the very low values of $\Delta S_d^{\ddagger}$ obtained. Indeed, the scale of the changes in $\Delta H_d^{\ddagger}$ and $\Delta S_d^{\ddagger}$ on going from homogeneous solution to the α-cages of sodium zeolite Y is such that it is easy to imagine that, under slightly different circumstances, a zeolite cavity could easily fail to act catalytically at all, any decrease in $\Delta H^{\ddagger}$ being overcome by an even larger decrease in $T\Delta S^{\ddagger}$. It is clear that the CO-inhibited reactions, which we have rather loosely called dissociative so far, exhibit aspects of associative reactions (with ZO···Mo bond making) and S_E3' reactions (with the development of the $ZONa^+\cdots(OC)Mo(CO)\cdots Na^+OZ$ interaction).

The rates of the associative reactions in the nr's are, by contrast, not very different from those of comparable reactions in homogeneous solution. Activation parameters for reaction with $P(n\text{-}Bu)_3$ in xylene[29] lead to a value of $k_a(P(n\text{-}Bu)_3) = (4 \pm 1) \times 10^{-5}$ M^{-1} s^{-1} at 65.8 °C, and reaction with PMe_3 should be 2–3 times faster than this because of its greater basicity and smaller size.[30,34] This leads to a specific rate of ca. 10^{-4} s^{-1} with 1 mol/L of PMe_3 in homogeneous solution, as compared to a specific rate of 7×10^{-5} s^{-1} with 1 PMe_3 molecule/nr. Indeed, the second-order rate constant for reaction in solution can be expressed as ca. 2×10^{-4} s^{-1} (molecule/nr volume)$^{-1}$ by using a volume of ca. 10^{-24} L for the nr together with Avogadro's number, so the rate constant for reaction with Pc in the zeolite is actually somewhat *smaller* than that in solution when comparable units are used.

The value of $\Delta H_a^{\ddagger}$ for the associative reactions in the zeolite results from the temperature dependence of the sum of two different second-order reactions (with Pc and Pp), but the value is still useful for comparative purposes. Because the Pc molecules are more strongly bonded in the zeolite than the Pp molecules, we would expect $\Delta H_a(Pc)^{\ddagger}$ to be greater than $\Delta H_a(Pp)^{\ddagger}$, so that the former will be clearly greater than the value for reaction in solution (Table VIII). This must be offset by a somewhat greater probability of reaction in the zeolite, though this effect is not nearly as large as one might expect from the propinquity of the $Mo(CO)_6$ and PMe_3 molecules in the nr's, which would seem to remove the necessity for the diffusion that is required in solution. We must conclude that reaction within the nanoreactor remains quite improbable, even when sufficient activation enthalpy is provided. We believe that this may be because of the unfavorable orientation of the chemisorbed PMe_3 molecules with respect to the $Mo(CO)_6$, with the Me groups, and not the P atom, being directed toward the $Mo(CO)_6$. In other words, when the $Me_3P\cdots Na_{II}^+OZ$ bond is broken, it can be very rapidly re-formed compared with its rate of rotation to allow the P atom to be directed toward the $Mo(CO)_6$ molecule, and the advantage of the closeness of the reactants in the α-cages is thereby much reduced. These rather subtle considerations suggest that the balance between dissociative and

(33) Ozin, G. A.; Özkar, S. *Chem. Mater.* **1992**, *4*, 511.
(34) Liu, H.-Y.; Eriks, K.; Prock, A.; Giering, W. P. *Organometallics* **1990**, *9*, 1758.

associative processes might be very dependent on the nature of the cation in the zeolite host, the Si:Al ratio, and the zeolite structure type. They could also explain the absence of a clean reaction with PEt_3, where rotation of the freed nucleophile may be more difficult.

The similarity of the rates of the associative reactions of $Mo(CO)_6$ with Pc and Pp molecules is also of interest. Since $\Delta H_a(Pc)^\ddagger$ must be greater than $\Delta H_a(Pp)^\ddagger$, this implies that the probability of reaction with Pp molecules is lower to a compensating extent in spite of the low absolute probability of reactions with Pc discussed above. The slightly greater distance of the Pp molecules from the $Mo(CO)_6$ and/or details of the anchoring of the Pp molecules must therefore have a significant effect on the probability of the reaction. It is clear from this discussion that the separate determination of $\Delta H_a(Pc)^\ddagger$ and $\Delta H_a(Pp)^\ddagger$ remains an important priority for further study, since it would provide a quantitative measure of the different strengths of adsorption of the two types of PMe_3 molecules, as well as of the different probabilities of reaction involved.

The relatively high value of $\Delta H_a^\ddagger$ for the associative reaction with Pc molecules in the α-cages of sodium zeolite Y compared with that in homogeneous solution can easily be ascribed in large part to the lower chemical potential of the chemisorbed PMe_3 molecules. The effect of the nr's on the $Mo(CO)_6$ partner in these reactions is harder to envisage. The approaching PMe_3 molecule should increase the net electron density on the Mo atom in the transition state, and it should consequently increase the interaction of the transition state with the Na_{II}^+ ions (provided steric effects due to the increased coordination number in the complex do not prevent this greater anchoring). Such an effect would decrease the value of $\Delta H_a^\ddagger$ (but make $\Delta S_a^\ddagger$ more unfavorable), thus offsetting the effect of the lower chemical reactivity of the Pc molecules. The overall effect of the nr's is therefore the result of a combination of opposing ground- and transition-state effects that are presently difficult to unravel in any clear and quantitative way.

3.2 Cooperative Effects on the Dissociative Reaction. The rates of the dissociative path are clearly and quite strongly dependent on the extent of loading of $Mo(CO)_6$, PMe_3, and ^{13}CO, with values of $\Delta G_d^\ddagger$ increasing linearly with loading by 3.2 ± 0.4 kJ mol^{-1} (molecules of $Mo(CO)_6/\alpha$-cage)$^{-1}$, 1.04 ± 0.23 kJ mol^{-1} (molecules of PMe_3/α-cage)$^{-1}$, and 1.27 ± 0.07 kJ mol^{-1} (100 Torr of $^{13}CO)^{-1}$, respectively (Figure 10). Although significant, these effects are relatively small compared with the overall effect, ca. 20 kJ mol^{-1}, of the nr on the value of $\Delta G_d^\ddagger$ compared with homogeneous solution, and they represent, therefore, a relatively minor perturbation. For this reason their explanation is less easy to ascertain, especially since we know the effects only on $\Delta G_d^\ddagger$ and not on $\Delta H_d^\ddagger$ and $\Delta S_d^\ddagger$ separately. However, it does seem likely that, when PMe_3 and ^{13}CO become attached to the Na^+ ions in the α-cages, the consequent negative charge buildup on the Na^+ could be transmitted through the zeolite framework to the Na^+ ions that will be used to anchor the $\{Mo(CO)_5\cdots CO\}^\ddagger$ transition state. This will weaken that anchoring and so slow down the rates. However, the same transmitted effect might seem likely to strengthen the developing $ZO\cdots Mo(CO)_5$ bond, and the balance of these two effects is hard to estimate. Indeed, these perturbing effects are small enough that they could even result from a decrease in $\Delta H_d^\ddagger$ that is more than offset by a larger decrease in $T\Delta S_d^\ddagger$, careful and precise studies of the temperature dependence of these perturbations being required to resolve this question.

The quite strongly inhibiting effect of increased $Mo(CO)_6$ loading on the reactions with PMe_3 is surprising at first sight because the $Mo(CO)_6$ molecules have been supposed to be rather weakly anchored in the presence of PMe_3 molecules. If they are only weakly bonded within the α-cage, then it would be incongruous for them to transmit a rather large effect (ca. 3× larger than the equivalent number of chemisorbed PMe_3 molecules) throughout the zeolite framework. This surprising observation may reveal a somewhat stronger interaction of the $Mo(CO)_6$ molecules with the Na_{II}^+ ions in the nr than is indicated by the spectroscopic techniques, which may be rather insensitive to these interactions, compared with the kinetic probe. The strength of the interaction is also indicated by the fact that the introduction of $Mo(CO)_6$ molecules into the zeolite can displace chemisorbed PMe_3 molecules previously loaded into the α-cages. The accelerating effect of the zeolite must then be ascribed to the development of an even stronger anchoring of the $\{Mo(CO)_5\cdots CO\}^\ddagger$ transition state compared with a significant but lower anchoring of the $Mo(CO)_6$ in its ground state, and this highlights the suggested contribution of $ZO\cdots Mo$ bonding in the transition state.

The range of operation of these loading effects can also be inferred from the kinetics data. The plots of $\Delta G_d^\ddagger$ vs PMe_3 and $P(^{13}CO)$ in Figure 10 clearly converge to the same value (104.1 ± 4.4 kJ mol^{-1} and 104.4 ± 0.2 kJ mol^{-1}, respectively), and this implies that the transmitted effects are operative down to quite low loadings and that they can therefore be exerted over quite long ranges throughout the zeolite host lattice.

Another important observation is that the effect of increased PMe_3 loading can be extrapolated from $\overline{PMe_3} = 2.7$ to $\overline{PMe_3} = 4$ molecules/α-cage to meet with the extrapolation to [Pp] = 0 of the associative reaction as shown in Figure 9. This means that it is not only chemisorbed PMe_3 molecules in the nr's but also Pc′ molecules in neighboring empty α-cages that affect the rates.

It can also be concluded, though perhaps rather tentatively, that Pp molecules do not have any or as strong an inhibiting effect on the rates. The second-order rate constant $k_a(Pp)$ obtained from reactions in the absence of CO (Figure 9) is derived from k_{obsd} values which are the sum of k_d, $2k_a(Pc)$, and $k_a(Pp)[Pp]$, on the assumption that k_d remains constant when [Pc] and [Pc′] are constant but [Pp] increases. If the increase in concentration of Pp molecules were to exert a growing and pronounced retarding effect on k_d, then the value of $k_a(Pp)$ would be much higher than that estimated, yet it is indistinguishable from that obtained under 650 Torr of CO, where no dissociative reaction is occurring.

The inhibiting effect of increased $Mo(CO)_6$ loading on the dissociative reaction also seems to operate even at very low loadings, down to 0.04 molecule/α-cage (Figure 10c). This implies a very long range transmitted effect from one nr, across as many as ca. 25 empty α-cages, to a different nr. These long-range effects are small but are significant and detectable because of the sensitivity of the kinetic probe. Thus the effect transmitted across 10 α-cages is ca. 0.3 kJ mol^{-1} in $\Delta G_d^\ddagger$, but this corresponds to a clearly detectable change of rate (Figure 10c and 13). The question of whether the product molecules exert a different transmitted effect than do reactant $Mo(CO)_6$ molecules themselves can be considered by reference to the linearity of the rate plots. Any pronounced difference could lead to curved rate plots as the reactant:product ratio changed, so we might conclude that the difference in the transmitted effects cannot be appreciable. Alternatively, and perhaps more probably, the greater basicity of the CO ligands in *cis*-$Mo(CO)_4(PMe_3)_2$ that is indicated by the DOR-NMR data described above could be balanced by the fact that, for every product *cis*-$Mo(CO)_4(PMe_3)_2$ molecule formed during the reaction, there is a corresponding loss of two PMe_3 molecules in the same nr.

The increase of the rate of CO dissociation by a factor of ca. 20 when two molecules of $Mo(CO)_6$ are present in 40% of the nr's is remarkable. Clearly one $Mo(CO)_6$ molecule can considerably enhance the reactivity of the other toward CO dissociation. Figure 3D shows a Chem-X space-filling model, which serves to illustrate the close proximity, orthogonal configuration, and likely intermolecular interactions that exist for the site II Na^+ anchored $Mo(CO)_6$ molecules cohabitating in an α-cage of sodium zeolite Y. This evidently bimolecular type of activation can be understood in terms of the formation, during CO loss, of dimeric species that can involve either Mo–CO···Mo bonding or even Mo–Mo bond formation and CO bridging in an intermediate such as I, both Mo atoms retaining their 18-electron configuration in these dimers.[35] Although this rate enhancement is very substantial, it

(35) This bimolecular interaction is reminiscent of that observed between $Mn_2(CO)_{10}$ and $Re_2(CO)_{10}$ in their scrambling reaction to form $MnRe(CO)_{10}$.[36]

can essentially be eliminated by 650 Torr of applied pressure of CO (Table V and Figure 13).

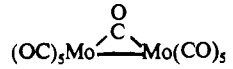

I

3.3 Cooperative Effects on the Associative Reactions. The associative path that involves reaction of $Mo(CO)_6$ with Pp molecules is clearly affected by the detailed environment to a negligible extent. Thus, the linearity of the increase of k_{obsd} with [Pp] shows that k_a(Pp) is independent of the amount of Pp present (Figure 9). The essentially identical values of k_a(Pp) found at low $Mo(CO)_6$ loadings and in the absence or presence of 650 Torr of CO (Figure 9) show that CO also has no appreciable effect on k_a(Pp). The still-unchanged value of k_a(Pp) obtained under 650 Torr of CO and in the presence of $Mo(CO)_6$ loadings that vary from 0.48 to 1.0 $Mo(CO)_6$ molecule/nr (runs 48, 50, and 51 in Table V, and Figure 13) shows a similar independence of the presence of varying amounts of $Mo(CO)_6$.[37]

These observations show that loading effects on the chemical reactivity of the Pp nucleophiles are generally unimportant, just as the loading of Pp molecules has a negligible effect on the rates of the dissociative reaction. However, the loading effects on the chemical reactivity of the $Mo(CO)_6$ molecules toward associative reactions appear also to be small, and this seems to be in conflict with the conclusion reached earlier that ground-state $Mo(CO)_6$ molecules in the α-cages are anchored sufficiently strongly for them to have strong effects on the dissociative reactions in other nanoreactors. If they are quite strongly anchored, then one might expect their anchoring to be affected by the loading, with consequent effects on their reactivity toward associative reactions as well, although the effects on dissociative and associative reactions do not have to be the same.

The associative path that involves reaction with Pc molecules also shows negligible, or at least small, loading effects. Thus, (i) although only two points are available, the value of k_a(Pc)[Pc] almost doubles from [Pc] = 1 to 2 molecules/nr; (ii) the value of k_a(Pc)[Pc] ([Pc] = 2 molecules/nr) remains constant even when the number of Pc′ molecules in neighboring "empty" cages increases from 2 to 4; (iii) the value of k_a(Pc)[Pc] decreases only slightly (by 35%) as the $Mo(CO)_6$ loading increases from 0.03 to 1 molecule/nr; (iv) the values of k_a(Pc) determined under 650 Torr of CO can be successfully used to estimate the value of k_d from k_{obsd} when reactions are carried out in the absence of CO; and (v) the values of k_a(Pp) can be estimated successfully by assuming that k_a(Pc) does not change with changing loadings of Pp molecules. It seems clear, therefore, that k_a(Pc) is essentially unaffected by the number of PMe_3 molecules in the nr or in neighboring α-cages, or by the number of Pp molecules present. It is not affected by the presence or absence of CO, and it is only quite slightly affected by the variation in the amount of $Mo(CO)_6$ present.

The almost complete absence of loading effects on these associative reactions has to be considered in light of the fact that the overall effect of encapsulation in the α-cages is small (see end of section 3.1). Since the large effect of the α-cages on the dissociative process is only affected by loading changes to a relatively small extent, we might expect the much smaller overall effect of the zeolite framework on the associative paths to be itself much less affected by loading changes.

3.4 The Homogeneity of the Loading of Zeolite Guest Molecules. The hypothesis of homogeneous distributions of the $Mo(CO)_6$ and PMe_3 molecules that was made in order to estimate the numbers of Pc and Pp molecules in the α-cages or twelve-ring windows does seem to be supported by the kinetics data. The rather sharp transition between the combined dissociative and associative (with Pc) reactions to the associative reaction with Pp molecules, shown in Figure 9, and the almost equally sharp transition between associative reaction with Pc and Pp molecules under 650 Torr of CO, also shown in Figure 9, both suggest that Pp molecules do not appear in the twelve-ring windows until all the available chemisorption sites are filled, and this is to be expected from the considerably greater strength of bonding of the Pc molecules. The most dramatic indication of the homogeneity of the distribution of the $Mo(CO)_6$ molecules is provided by run 45, which involves an average of ca. 1 $Mo(CO)_6$ molecule/α-cage. If these were distributed statistically, with 25% of the α-cages unoccupied by $Mo(CO)_6$, 50% occupied by 1 $Mo(CO)_6$, and 25% occupied by 2 $Mo(CO)_6$, then a very large enhancement of the rate would be expected in view of the result for run 46, where at least 40% of the nanoreactors are doubly occupied and a greatly enhanced rate is observed. Contrary to this, run 45 proceeds rather more slowly than predicted, even for homogeneous loading, and possible reasons for this were discussed above.

Not only do the sharp transitions in kinetic behavior provide evidence for homogeneity but they also act as "end points" in kinetic titrations of different binding sites in the zeolite. The fact that the transitions do occur rather close to appropriate integral loading numbers is of considerable significance.

3.5 The Relative Yields of $Mo(CO)_5(PMe_3)$ and *cis*-$Mo(CO)_4(PMe_3)_2$. The formation of *cis*-$Mo(CO)_4(PMe_3)_2$ as the only product detectable when reaction occurs with PMe_3 in the absence of CO is compatible with the dissociative reaction sequences shown in eqs 2–5, but it is not at first sight easily reconciled with the fact that the reactions are simultaneously proceeding at comparable rates by an associative path. The latter would be expected to lead only to $Mo(CO)_5(PMe_3)$.

When reactions are carried out in the presence of Pc molecules only, the yield of $Mo(CO)_5(PMe_3)$ is found to be constant at 30–40% over the P(CO) range 50–650 Torr. The presence of CO could be envisaged as allowing the formation of $Mo(CO)_5(PMe_3)$ via the dissociative path, but the contribution of this path to the overall reaction is effectively quenched by $P(CO) \geq 400$ Torr, so that the associative reaction with Pc molecules is still leading to substantial yields of *cis*-$Mo(CO)_4(PMe_3)_2$.

Reaction with $\overline{PMe_3} = 6$ molecules/α-cage still leads only to *cis*-$Mo(CO)_4(PMe_3)_2$ in the absence of CO when ca. one-third of the reactions are proceeding by the associative path with Pp. Over the range $P(CO) = 50$–650 Torr the yield of $Mo(CO)_5(PMe_3)$ increases from ca. 20 to 90%, a quite different behavior from that with Pc molecules described above.

No studies of the equilibria between $Mo(CO)_5(PMe_3)$ and *cis*-$Mo(CO)_4(PMe_3)_2$ under CO in the presence of Pc or of Pc and Pp molecules have yet been undertaken, and the effects of widely different loadings on the rates of reactions of $Mo(CO)_5(PMe_3)$ have yet to be investigated, so the observed pattern of yields under CO may be the result of thermodynamic contributions. The latter would not affect reactions in the absence of CO, however, and some intriguing questions therefore remain.

4. Summary of the Kinetic and Mechanistic Behavior. The reactions in $Na_{56}Y$ are very clean, and the kinetics are generally very reproducible, showing that similar studies of a wide range of reactions of organometallic compounds should be feasible and informative. Further:

(i) As in homogeneous solution, reactions proceed by CO-dissociative paths and, with the strong nucleophile PMe_3, by associative paths.

(36) Marcomini, A.; Poë, A. J. *J. Am. Chem. Soc.* **1983**, *105*, 6952.

(37) Although pseudo-first-order conditions are not maintained throughout these reactions, this can be shown to have relatively little effect, especially if the Pc molecules are concluded not to diffuse through the matrix during the reaction. If they do not, then the depletion of Pc molecules throughout the reactions will occur only in those nr's where a reaction has already occurred, and there will be no effect on the probability of reaction of $Mo(CO)_6$ molecules in other nr's. Because the Pp molecules are probably in the twelve-ring windows between α-cages that can both be occupied when the $Mo(CO)_6$ loading is high, the availability of Pp molecules will decrease somewhat during the reaction, but the effect of this on k_{obsd} for runs 48, 50, and 51 will be $\leq$10%, and the effect on k_a(Pp), negligible. Run 52 is exceptional in that 86% of the nr's contain two $Mo(CO)_6$ molecules and only 14% contain one, together with two Pc molecules. The proportion of reaction that involves Pc molecules is therefore reduced, and the proportion proceeding via other reaction paths is correspondingly greater. This leads to a rate constant for reaction with Pp molecules that is apparently high, and it seems very likely that the bimolecular activation of the dissociative path when two $Mo(CO)_6$ molecules are in the same *nr* may not be completely quenched by 650 Torr of applied CO pressure.

(ii) The rate of the dissociative path is accelerated at 65.8 °C by ca. 10^3 (20 kJ mol^{-1} in $\Delta G_d^{\ddagger}$) compared with the rate in homogeneous solution.

(iii) This acceleration is due to a large decrease in $\Delta H_d^{\ddagger}$ which is considerably offset by a much less favorable value of $\Delta S_d^{\ddagger}$.

(iv) The acceleration can be ascribed to transition-state stabilization caused by greater anchoring of the transition state by two site II Na^+ ions, probably assisted by partial bonding between a framework oxygen and the Mo atom as the CO ligand leaves.

(v) The CO-dissociative path is significantly and systematically retarded by increased $Mo(CO)_6$ and PMe_3 loading and, in the case of the CO-exchange reaction, by increased pressures of ^{13}CO. These effects can be quite long range but are relatively small compared to the overall acceleration by the $Na_{56}Y$ host lattice.

(vi) There are two associative paths, one with chemisorbed and one with physisorbed PMe_3, and their rates are not very different from those in homogeneous solution. Although the probabilities of these paths are significantly greater than in homogeneous solution, the effect of preassembly of the reactants in the zeolite is not as large as might be expected, and this can be understood on the basis of unfavorable relative conformations of the $Mo(CO)_6$ and chemisorbed PMe_3 molecules in the nr's.

(vii) The associative reactions are not appreciably affected by different loadings of $Mo(CO)_6$ or PMe_3 or by different applied pressures of CO.

Concluding Remarks

This investigation has yielded the first quantitative measurements of the influence of an internal "perfect" surface of a zeolite host lattice on the reactivity of encapsulated guests. It has unveiled an appealing picture of the α-cage nanoreactor as a rigid macrospheroidal, multisite, multidentate alkali metal cavitate (a zeolate ligand), the effect of which can be to enhance CO-dissociative reactivity by transition-state stabilization. Apart from providing information on the mode of activation of an organometallic system, the results show that the kinetics of a given reaction can be used as one more probe, and quite a sensitive one, of the nature of a zeolite and the transmission of effects through it.

The models proposed to explain the enhanced reactivity should aid in the design of further experiments and the interpretation of cation and framework anchoring, Si:Al ratio, and guest loading effects on activation parameters and reaction mechanisms of other reactions in zeolites compared with those in homogeneous solution or other matrix environments.

Quantitative experiments of this kind are expected to be of great value in understanding the intimate details of size- and shape-selective catalytic reactions, the origin of adsorption, host–guest inclusion and molecular recognition phenomena, and the parameters that control a range of intrazeolite synthetic and self-assembly processes that are basic to the preparation of new solid-state nanoporous materials of interest in, for example, chemoselective sensing, quantum electronics, nonlinear optics, photonics, information storage, and artificial photosynthesis.[38]

Acknowledgment. The generous financial assistance of the Natural Sciences and Engineering Research Council of Canada (G.A.O., A.J.P.) is sincerely appreciated. H.O.P. expresses her gratitude to Conselho Nacional de Desenvolvimento Cientifico e Tecnologico (Brazil) for a graduate scholarship and to Professor Eduardo J. S. Vichi for his support and for giving her the opportunity to work in Toronto. We also wish to acknowledge the invaluable assistance of Professor P. M. Macdonald with MAS-NMR, Mr. R. Jelinek and Professor A. Pines with DOR-NMR, and Dr. R. Prokopowicz with EXAFS experiments and data analysis. The EXAFS measurements were carried out at the National Synchrotron Light Source, Brookhaven National Laboratories, which is supported by the U.S. Department of Energy, Division of Materials Sciences and the Division of Chemical Sciences. All of us are indebted to Professor Özkar for help in the early stages of this work and for his helpful comments on the manuscript, and to Professor Vichi for his original suggestion (to A.J.P. in 1986) that such work should be initiated.

(38) Ozin, G. A. *Adv. Mater.* **1992**, *4*, 612.